Fluid Phase Equilibria 358 (2013) 250–271

Contents lists available at ScienceDirect

Fluid Phase Equilibria

journal homepage: www.elsevier.com/locate/fluid

Characterization of reservoir fluids using an EOS based on perturbation from *n*-alkanes

Ashutosh Kumar, Ryosuke Okuno*

School of Petroleum Engineering, University of Alberta, Canada

ARTICLE INFO

Article history:
Received 30 June 2013
Received in revised form 26 August 2013
Accepted 28 August 2013
Available online 6 September 2013

Keywords:
Equations of state
Fluid characterization
Petroleum reservoir fluids
Gibbs free energy
Volume shift

ABSTRACT

Characterization of reservoir fluids using a cubic equation of state (EOS) is conducted under unavoidable uncertainties in pressure–temperature–composition (P–T–x) space. The implicit, non-linear relationship between phase behavior predictions and adjustment parameters also makes fluid characterization non-unique and subjective. Although P–T–x space that phase behavior spans is continuous, different characterization methods have been proposed for different types of reservoir fluids.

In our previous research, a method was developed for heavy-oil characterization using the Peng–Robinson (PR) EOS with the van der Waals mixing rules without volume shift. Uncertainty issues in heavy-oil characterization were addressed based on the concept of perturbation from *n*-alkanes (the PnA method). Pseudo components were initially assigned critical parameters that were optimized for *n*-alkanes in terms of liquid densities and vapor pressures using the PR EOS. The optimized reference values allowed for well-defined directions for perturbation of pseudo components' critical parameters to match available experimental data. The robust regression algorithm required only three perturbation parameters.

In this paper, we extend the PnA method to lighter fluids, such as gas condensates, volatile oils, and near-critical fluids. The main novelty of the new PnA method is that it considers proper interrelationship ($\psi = a/b^2$) between the attraction (a) and covolume (b) parameters of pseudo components. The regression algorithm developed in this research controls the trend of the ψ parameter with respect to molecular weight using a fourth adjustment parameter γ. The ψ and γ parameters become more important for characterizing lighter fluids. For extra heavy oils, the new PnA method naturally reduces to the previous PnA method, where γ is zero.

Case studies using 77 different reservoir fluids demonstrate the universal applicability, reliability, robustness, and efficiency of the new PnA method. The fluids used consist of 34 heavy and black oils, 12 volatile oils, and 31 gas condensates. Six fluids are near critical among them. The PnA method controls phase behavior predictions monotonically with parameter adjustments and systematically in P–T–x space. This is demonstrated by quantitative prediction of condensation/vaporization behavior of gas condensates and light oils and minimum miscibility pressures for various oil displacements. The PnA method requires no change in the thermodynamic model used, i.e., it can be readily implemented in existing software based on the PR EOS with the van der Waals mixing rules.

We also explain how volume-shift parameters affect compositional phase behavior predictions when used as regression parameters in fluid characterization. The PnA method uses no volume shift, and properly couples volumetric and compositional phase behaviors.

1. Introduction

Compositional modeling is widely used to simulate enhanced oil recovery and recovery of gas condensates and volatile oils. Reliability of compositional simulation can depend significantly on the phase behavior model used in the simulation. Cubic equations of state (EOSs), such as the Peng–Robinson (PR) EOS [1,2], are used to calculate phase behavior in compositional simulation. These cubic EOSs along with the van der Waals mixing rules give reasonable accuracy and high computational efficiency for vapor–liquid equilibrium of reservoir fluids.

Characterization of reservoir fluids using a cubic EOS is conducted based on experimental data available, which typically consist of composition analysis and pressure–volume–temperature

* Corresponding author at: 3-114 Markin/CNRL Natural Resources Engineering Facility, University of Alberta, Edmonton, Alberta T6G 2W2, Canada. Tel.: +1 780 492 6121; fax: +1 780 492 0249.
E-mail addresses: rokuno@ualberta.ca, okuno@alumni.utexas.net (R. Okuno).

0378-3812/$ – see front matter © 2013 Elsevier B.V. All rights reserved.
http://dx.doi.org/10.1016/j.fluid.2013.08.035

Nomenclature

Roman Symbols

a	attraction parameter in a cubic equation of state
A	aromatic
AD	average deviation
AAD	average absolute deviation
b	covolume parameter in a cubic equation of state
c	Peneloux volume-shift parameter for N_C components
C_{PEN}	Peneloux volume-shift parameter
d	gradation constants
f_{avg}	average of perturbation parameters as defined in Eq. (17)
f_{dis}	Chi-squared distribution function defined in Eq. (5)
f_m	perturbation factor for the m parameter
f_P	perturbation factor for critical pressure
f_T	perturbation factor for critical temperature
$\Delta_{mix}\underline{G}$	molar Gibbs free energy change on mixing
g	dimensionless molar Gibbs free energy change on mixing
k	iteration number
k	binary interaction parameter matrix with elements k_{ij} for components i and j
m	parameter in the Peng–Robinson EOS (1978) defined in Eqs. (9) and (10)
N_C	number of components
P	pressure, bar
p	parameter in the Chi-squared distribution
P_C	critical pressure, bar
$\mathbf{P_C}$	critical pressure vector for N_C components
R	universal gas constant
S	parameter in the Chi-squared distribution
T	temperature, K
T_C	critical temperature, K
$\mathbf{T_C}$	critical temperature vector for N_C components
x	mole fraction vector for the liquid phase
y	mole fraction vector for the gaseous phase
z	overall composition vector
z_L	mole fraction of methane in fluid
z_I	sum of mole fractions of non-C_{7+} excluding methane
z_H	mole fractions of C_{7+}

Abbreviations

°API	API (American Petroleum Institute) gravity
BIP	binary interaction parameter
CN	carbon number
$CM_{w/o}V$	conventional (characterization) method without volume shift
CM_wV	conventional (characterization) method with volume shift
EOS	equation of state
MMP	minimum miscibility pressure, bars
MW	molecular weight, gm/mol
PC	pseudo-component
PNA	paraffin–napthene–aromatic
PR	Peng–Robinson
P–T–x	pressure–temperature–composition

Greek symbols

β	vapor molar phase fraction
ε	T_C, P_C, and ω consistency function defined in Eq. (12)
Γ	Gamma function
$\bar{\phi}_i$	fugacity coefficient of component i in a mixture
ϕ_i	fugacity coefficient of pure component i
γ	gradation parameter
Ω_a	constant term in the attraction parameter of a cubic EOS
Ω_b	constant term in the covolume parameter of a cubic EOS
ψ	a_i/b_i^2 defined in Eq. (13) for the PR EOS
θ	parameter as defined in Eq. (17)
ω	acentric factor vector for N_C components

Subscripts/superscript symbols

w	with (volume shift)
w/o	without (volume shift)
L	liquid phase
V	gaseous phase

(*PVT*) data. Compositional analysis provides the concentrations of light components (e.g., up to C_6) and a plus fraction (e.g., C_{7+}), and the density of the plus fraction at atmospheric conditions. The compositional uncertainty left as a plus fraction becomes higher for heavier fluids [3]. *PVT* measurements are performed at selected pressure–temperature–composition (P–T–x) conditions. It is difficult to predict and cover reservoir P–T–x conditions, which result from fluid and energy flow in a heterogeneous reservoir, in laboratory measurements. Thus, reservoir fluid characterization is performed under unavoidable uncertainties in composition and phase behavior data in P–T–x space. However, theory has not been established, based on which engineers can perform reliable fluid characterization using a cubic EOS under such uncertainties.

A typical characterization process consists of four main steps [4,5] as follows:

Step 1. Estimation of a molar distribution with respect to molecular weight (MW) or carbon number (CN) to split the plus fraction into detailed components.
Setp 2. Estimation of properties for the detailed components such as critical temperature (T_C), critical pressure (P_C), critical volume (V_C), acentric factor (ω), and volume-shift parameters.
Step. 3 Grouping of the detailed components into fewer pseudo components.
Step 4. Regression of pseudo components' properties to match experimental data available.

The parameter regression in step 4 is often needed because steps 1–3 make certain assumptions causing deviations of predictions from actual phase behavior. For example, various correlations used in step 2 were developed for an EOS to reproduce the critical point and vapor pressure for the pseudo component of a given CN. Use of such correlations implicitly assumes a certain distribution of hydrocarbon types within that CN group (e.g., paraffins, naphthenes, and aromatics, or PNA distribution). Furthermore, unless volume shift is used, a cubic EOS is inaccurate in prediction of liquid densities even if accurate critical parameters and acentric factor are known and used [6–8].

Current best practice for step 4 is step-wise manual adjustment of parameters to match experimental data available. Simultaneous regression of various parameters using software as a black box is not recommended [3]. The adjustment parameters often used include T_C, P_C, V_C, ω, volume-shift parameters, and binary interaction parameters (BIPs) for pseudo components. Special care must be taken by experienced engineers to ensure physically acceptable trends of adjustment parameters with respect to MW or CN [9]. Even with this best practice, different fluid models are created

Steps	Input	Output
1. a and b for components	$(T_C, P_C, \omega)_i$	a_i, b_i
2. a and b for mixtures	Binary interaction parameters Mixing rules (e.g., van der Waals mixing rules)	a_m, b_m
3. Gibbs free energy	EOS (e.g., PR EOS)	Gibbs free energy
4. Compositional behavior (Flash calculation)	Temperature, Pressure, Composition	Phase compositions and amounts
5. Volumetric behavior	Volume-shift parameters	Volumetric phase properties

Fig. 1. Key steps of phase behavior calculation using a cubic EOS. Subscript *i* is the component index, and subscript *m* stands for mixture. *a* and *b* are the attraction and covolume parameters, respectively, for a cubic EOS. Regression in fluid characterization is conducted to match the volumetric (*PVT*) data with the volumetric phase behavior predictions calculated in step 5.

depending on selection of adjustment parameters and the adjustment amounts [10]. Since parameter adjustments are conducted with little physical justification, it is unclear whether the resulting fluid model is reliable when used in compositional simulation to predict oil and gas recovery.

The various issues described above indicate that theory should be developed for reliable fluid characterization using a cubic EOS under uncertainties in composition and phase behavior data in *P*–*T*–*x* space. One of the main reasons for the lack of theory is likely the unknown, implicit, non-linear relationship between phase behavior predictions and adjustment parameters such as T_C, P_C, V_C, ω, volume-shift parameters, and BIPs.

Different characterization methods have been proposed for different reservoir fluids [11–15]; for example, gas condensates [16–19], volatile oils [20,21], near-critical fluids [22–25], and heavy oils [26,27]. However, *P*–*T*–*x* space that phase behavior spans is continuous. Although size-asymmetric mixtures can be difficult to model using a cubic EOS with the van der Waals mixing rules [28,29], it will substantially benefit the petroleum industry if continuous modeling of all types of reservoir fluids becomes possible using a simple cubic EOS.

In our previous research, a method was developed for heavy-oil characterization using the PR EOS with the van der Waals mixing rules without volume shift [3]. Uncertainty issues in heavy-oil characterization were addressed based on the concept of perturbation from *n*-alkanes (the PnA method). Pseudo components were initially assigned T_C, P_C, and ω that were optimized for *n*-alkanes in terms of liquid densities and vapor pressures using the PR EOS [30]. The optimized reference values allowed for well-defined directions for perturbation of pseudo components' T_C, P_C, and ω to match *PVT* data available. We presented that robust regression using the PnA method required only three perturbation parameters to match volumetric and compositional phase behaviors with no volume shift. Important physical considerations used in the development of this PnA method include the following:

i. A PNA distribution of a plus fraction is interpreted as a perturbation from the limiting distribution of 100% *n*-alkanes.
ii. T_C and P_C of *n*-alkane are lower than those of other types of hydrocarbons (e.g., aromatics) within a given CN group. The trend is the other way around for ω.
iii. Without using volume shift, compositional and volumetric phase behaviors are properly coupled, and density data are effectively used.
iv. Pitzer's definition of ω [31,32] is satisfied for all pseudo components.

In this paper, we extend the PnA method to lighter fluids, such as gas condensates, volatile oils, and near-critical fluids. The main novelty of the new PnA method is that it considers proper variations of the attraction (*a*) and covolume (*b*) parameters of pseudo components based on the component distribution determined in the first characterization step. This physical consideration added is more important for lighter fluids. The new PnA method naturally reduces to the previous PnA method for heavy oils.

In the subsequent sections, we first discuss effects of volume shift on the Gibbs free energy and phase behavior predictions. The extension of the PnA method is then discussed in detail, where the importance of considering the interrelationship between the *a* and *b* parameters is explained. After that, the extended PnA method is applied to 77 different reservoir fluids, consisting of 34 heavy and black oils, 12 volatile oils, and 31 gas condensates. Six fluids are near critical among them. The universal applicability of the PnA method is conclusively shown in these applications.

2. Effect of volume-shift parameter regression on Gibbs free energy

Volume-shift parameters are widely used to correct volumetric predictions from a cubic EOS. Volume-shift parameters alter the form of a cubic EOS, but not the form of the fugacity equations. Therefore, volume shift can be performed separately from compositional behavior predictions [6,7]. Volume shift, however, affects compositional behavior predictions when used as regression parameters in fluid characterization as explained analytically and numerically in this section.

Kumar and Okuno [3] conducted comparisons of phase behavior predictions from two characterization methods using the PR EOS; one without volume shift and the other with volume shift. Although the two characterizations were equally accurate at the *P*–*T*–*x* conditions used in the regression, the latter gave erroneous phase behavior predictions at other *P*–*T*–*x* conditions. The deviation between the two characterizations was more significant for heavier oils since heavier oils tend to require more volume correction using the PR EOS.

Fig. 1 shows the main steps for phase behavior calculations using a cubic EOS. The first step is to calculate the *a* and *b* parameters for each component using T_C, P_C, and ω. The second step uses the mixing rules to calculate the *a* and *b* parameters for mixtures. Then, the Gibbs free energy is developed in *P*–*T*–*x* space using the EOS in the third step. Compositional phase behavior is determined by flash calculation or minimization of the Gibbs free energy at a given *T*, *P*, and overall composition ($\mathbf{z}$) in the fourth step. Volume shift, if used, corrects density predictions in the fifth step. Fluid characterization attempts to match volumetric (or *PVT*) data with volumetric predictions calculated in the fifth step. Fig. 1 clearly shows that volumetric phase behavior predictions depend on volume-shift parameters (if used), T_C, P_C, ω, and BIPs. Thus, two different characterizations that give the same volumetric predictions (fitted to *PVT* data) have different sets of T_C, P_C, ω, BIPs, and volume-shift parameters. It is evident in Fig. 1 that the relationship is significantly non-linear

Table 1
Ternary fluid using the conventional characterization method with/without volume shift in regression.

Components	Mole fractions	MW (g/mol)	PR EOS with volume shift				PR EOS without volume shift		
			T_C (K)	P_C (bars)	ω	CPEN (cc/mol)	T_C (K)	P_C (bars)	ω
L	0.4219	16.10	190.86	46.07	0.0089	−5.19	190.86	46.07	0.0089
I	0.0176	31.66	315.59	47.83	0.1065	−5.85	315.59	47.83	0.1065
H	0.5605	291.30	848.33	24.18	0.4373	−110.14	1022.44	19.48	0.5108
Temperature (K)			330.40						
Saturation pressure (bars)			196.48						
L = N_2 + CO_2 + C_1, I = C_2 + C_3, H = C_{4+}									

and implicit between phase behavior predictions and adjustment parameters in regression.

Compositional phase behavior predictions are determined by the parameters that form the single-phase Gibbs free energy (i.e., the Gibbs free energy calculated assuming a stable single-phase state even in multiphase regions). Let us consider two characterizations for a given fluid that yield the same volumetric predictions; one without volume shift and the other with volume shift. The parameter set is $(\mathbf{T_C}, \mathbf{P_C}, \boldsymbol{\omega}, \mathbf{k})^{wo}$ for the former, and is $(\mathbf{T_C}, \mathbf{P_C}, \boldsymbol{\omega}, \mathbf{k}, \mathbf{c})^{w}$ for the latter. The bold symbols, such as $\mathbf{T_C}$, $\mathbf{P_C}$, $\boldsymbol{\omega}$, and $\mathbf{c}$, indicate vectors consisting of N_C elements, where N_C is the number of components. $\mathbf{c}$ is a vector for N_C volume-shift parameters. $\mathbf{k}$ is a BIP matrix consisting of k_{ij} ($i = 1, 2, \ldots, N_C$, and $j = 1, 2, \ldots, N_C$). For the two cases, the dimensionless molar Gibbs free energy change on mixing, g, at a given T, P, and z is the following:

$$g^{wo} = \left(\frac{\Delta_{mix}G}{RT}\right)^{wo} = \sum_{i=1}^{N_C} \mathbf{z}_i \ln\left[\frac{z_i\bar{\varphi}_i(\mathbf{T_C}, \mathbf{P_C}, \boldsymbol{\omega}, \mathbf{k}, T, P, \mathbf{z})^{wo}}{\varphi_i(T_{Ci}, P_{Ci}, \omega_i, T, P)^{wo}}\right] \quad (1)$$

$$g^{w} = \left(\frac{\Delta_{mix}G}{RT}\right)^{w} = \sum_{i=1}^{N_C} \mathbf{z}_i \ln\left[\frac{z_i\bar{\varphi}_i(\mathbf{T_C}, \mathbf{P_C}, \boldsymbol{\omega}, \mathbf{k}, T, P, \mathbf{z})^{w}\exp(c_iP/RT)}{\varphi_i(T_{Ci}, P_{Ci}, \omega_i, T, P)^{w}\exp(c_iP/RT)}\right] = \sum_{i=1}^{N_C} \mathbf{z}_i \ln\left[\frac{z_i\bar{\varphi}_i(\mathbf{T_C}, \mathbf{P_C}, \boldsymbol{\omega}, \mathbf{k}, T, P, \mathbf{z})^{w}}{\varphi_i(T_{Ci}, P_{Ci}, \omega_i, T, P)^{w}}\right], \quad (2)$$

where φ_i is the fugacity coefficient for pure component i, and $\bar{\varphi}_i$ is the fugacity coefficient of component i in a mixture of overall composition $\mathbf{z}$. A single phase is assumed. Eqs. (1) and (2) show that two different sets of parameters give two different single-phase Gibbs free energy surfaces in P–T–x space.

For example, an oil is characterized as a ternary fluid using the PR EOS with and without volume shift as shown in Table 1. Actual compositional simulation studies often require a larger number of components. Use of only three components in this case study is to visually demonstrate the volume-shift effects in a simple manner. The ternary fluid consists of the L, I, and H components. All BIPs are zero for the two characterizations without loss of generality of the discussion. The two characterizations are equally accurate in calculation of the saturation pressure, 196.48 bars, at the reservoir temperature 330.4 K and oil densities at 276.3, 258.5, 223.6, 196.5, 175.2, 144.6, 103.0, 62.3, 41.0, and 7.1 bars at 330.4 K. However, the two characterizations have different properties for the H component.

Figs. 2 and 3 show g^{wo} and g^{w}, respectively, in composition space at 196.48 bars and 330.4 K based on the parameters given in Table 1 and Eqs. (1) and (2). The contour lines are equally spaced. The difference between g^{wo} and g^{w} is not obvious in the figures, but g^{wo} exhibits a deeper valley than g^{w}; there is no contour line corresponding to −0.8 for g^{w}, whereas the contour line corresponding to −0.8 is present for g^{wo}.

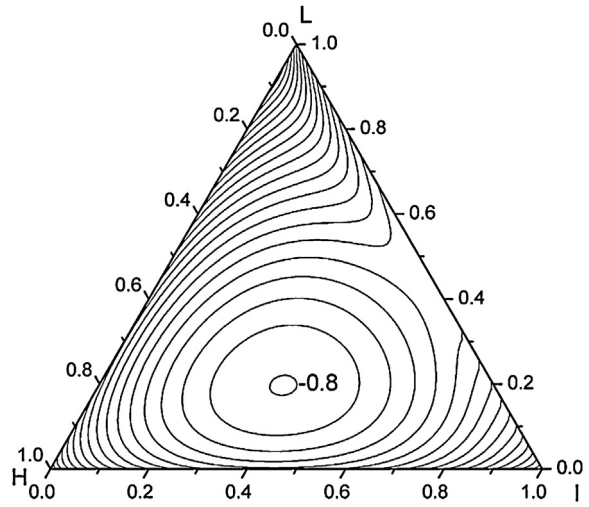

Fig. 2. Dimensionless molar Gibbs free energy change on mixing for the ternary fluid given in Table 1 at 330.4 K and 196.48 bars. Contour lines are drawn with the interval of 0.05 between −0.85 and 2.0. The PR EOS is used without volume shift.

Although volume shift does not change the form of fugacity equations, different set of parameters (the w and wo cases) results in different phase equilibria. For the two cases, the fugacity

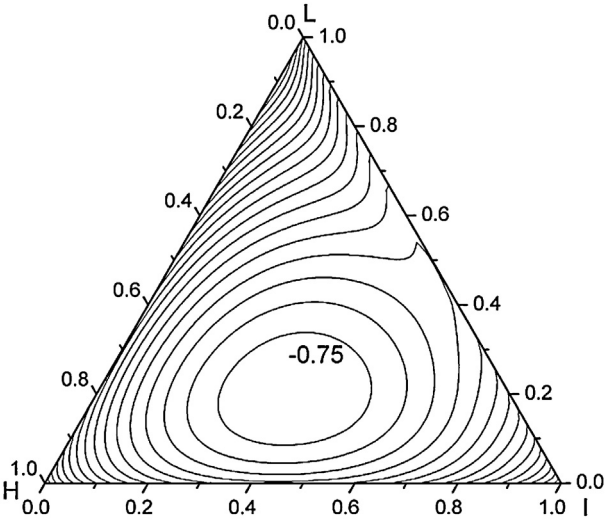

Fig. 3. Dimensionless molar Gibbs free energy change on mixing for the ternary fluid given in Table 1 at 330.4 K and 196.48 bars. Contour lines are drawn with the interval of 0.05 between −0.85 and 2.0. All the contour lines are higher than −0.8. The PR EOS is used. Volume shift parameters are used in regression.

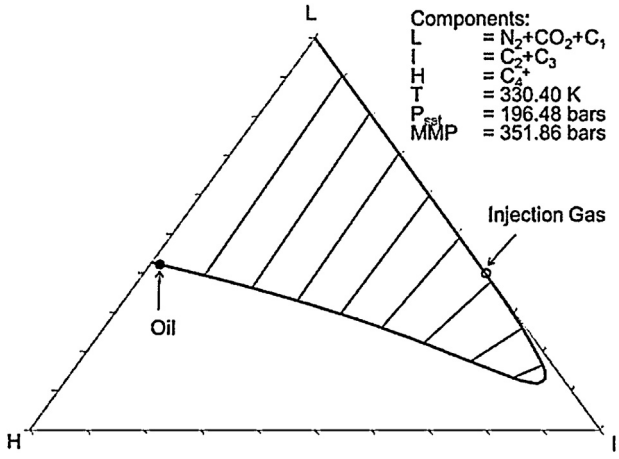

Fig. 4. Phase envelope for the ternary fluid given in Table 1. The PR EOS is used without volume shift. MMP calculated for the injection gas is 351.86 bars at 330.40 K.

equations for liquid–vapor (L–V) equilibrium at a given T, P, and overall composition is the following:

$$x_i^{wo}\bar{\varphi}_i^{L}(\mathbf{T_C}, \mathbf{P_C}, \boldsymbol{\omega}, \mathbf{k}, T, P, \mathbf{x})^{wo} = y_i^{wo}\bar{\varphi}_i^{V}(\mathbf{T_C}, \mathbf{P_C}, \boldsymbol{\omega}, \mathbf{k}, T, P, \mathbf{y})^{wo} \quad (3)$$

$$x_i^{w}\bar{\varphi}_i^{L}(\mathbf{T_C}, \mathbf{P_C}, \boldsymbol{\omega}, \mathbf{k}, T, P, \mathbf{x})^{w} = y_i^{w}\bar{\varphi}_i^{V}(\mathbf{T_C}, \mathbf{P_C}, \boldsymbol{\omega}, \mathbf{k}, T, P, \mathbf{y})^{w} \quad (4)$$

for all i, where $i = 1, 2, \ldots, N_C$, and $\mathbf{x}$ and $\mathbf{y}$ are the liquid and vapor phase composition vectors, respectively. Eqs. (3) and (4) are solved on the Gibbs free energy shown in Figs. 2 and 3. Results are presented in Figs. 4 and 5. The two-phase envelope without volume shift is larger than that with volume shift at 196.48 bars and 330.4 K in this case. The two characterizations give similar predictions near the oil composition. However, the difference becomes significant in the region away from the oil composition.

The different immiscibilities predicted can result in a large difference in the minimum miscibility pressure (MMP) for the two characterizations. For example, the MMP calculated at 330.4 K for the injection gas of 40% L and 60% I is 351.86 bars without volume shift and 250.75 bars with volume shift. This simple case study clearly shows that the effects of volume shift can be quite significant on oil recovery predictions. Since P–T–x conditions used in laboratory measurements cannot cover actual reservoir conditions encountered in reservoir processes, the volume-shift effects in P–T–x space should be considered in fluid characterization. The

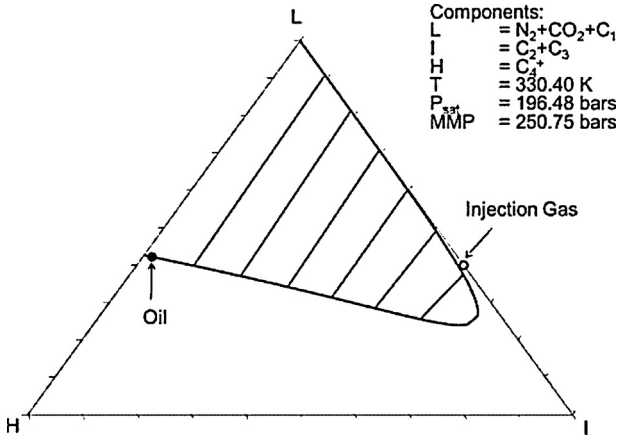

Fig. 5. Phase envelope for the ternary fluid given in Table 1. The PR EOS is used. Volume shift parameters are used in regression. Use of volume shift results in a two-phase envelope that is significantly smaller than that in Fig. 4. MMP calculated for the injection gas is 250.75 bars 330.40 K.

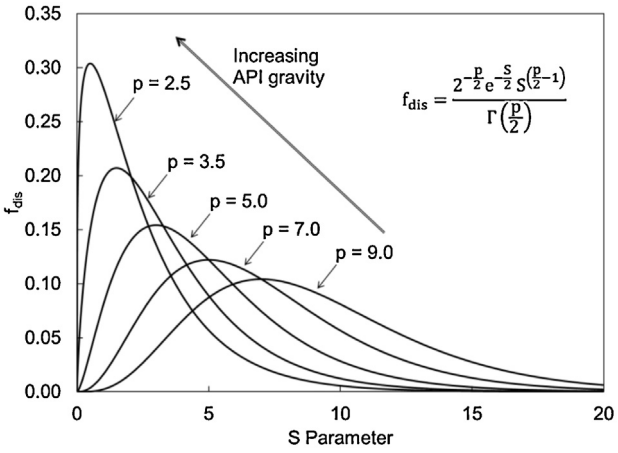

Fig. 6. Chi-squared distributions for different p values in Eq. (5). The p parameter controls the degree of skew and the size of effective composition space. A lighter fluid tends to have a smaller p value. For light fluids, the effective CN (or MW) range is small compared to heavy oils.

PnA method does not require volume shift to accurately predict volumetric and compositional phase behaviors as shown below. Therefore, the PnA method uses no volume shift, and properly couples the two types of phase behavior.

3. Extension of the perturbation from *n*-alkanes (PnA) method

The PnA method previously presented in Kumar and Okuno [3] successfully characterized heavy oils with the PR EOS as described in the introduction section. It required only three adjustment parameters f_T, f_P, and f_m to perturb T_C, P_C, and ω of pseudo components, respectively. The f_m perturbation parameter was used for the m parameter, a one-to-one function of ω used in the temperature-dependent term in the attraction term of the PR EOS. The perturbations were performed in well-defined directions from the n-alkane values of Kumar and Okuno [30]. A single value for each of the three adjustment parameters was successfully applied for all pseudo components for heavy-oil characterization.

In this section, the PnA method is extended to characterize other types of reservoir fluids without loss of simplicity. A fourth adjustment parameter is introduced to consider proper trends of the attraction and covolume parameters of the PR EOS with respect to MW (or CN) depending on the overall composition of the fluid to be characterized. The main novelty of this research lies in here.

3.1. Overall composition

The Chi-squared distribution function is used in the composition characterization step in the PnA method. More complicated functions like the gamma (Γ) distribution function can also be used. However, the Chi-squared distribution function can characterize the degree of skew, which is the key information required in the new PnA method, using the p parameter in

$$f_{dis} = \frac{2^{-(p-2)}e^{-(s-2)}S((p-2)-1)}{\Gamma(p-2)} \quad (5)$$

Eq. (5) expresses the probability density for the S variable, which is MW or CN in the context of composition characterization. The p parameter increases with decreasing API gravity in general. Its practical values range between 2 and 10 [33,34]. Fig. 6 shows Chi-squared distributions for different p values. The compositional characterization method using Eq. (5) is described in detail in Quiñones-Cisneros et al. [34], and is not duplicated here.

3.2. Critical parameters for n-alkanes and their internal consistency

A plus fraction contains a variety of compounds, such as paraffins, naphthenes, and aromatics (PNA). Conventional characterization methods assume implicitly a certain PNA distribution in their critical parameter estimation as described in the introduction section. In the PnA method, the PNA distribution of a plus fraction is initially set to be the limiting distribution of 100% n-alkanes, and then characterized explicitly in the regression algorithm. Thus, pseudo components are initially assigned the n-alkane values for T_C, P_C, and m based on the correlations of Kumar and Okuno [30]. The MW in the correlations was augmented by perturbation parameters f_T, f_P, and f_m in Kumar and Okuno [3];

$$T_C = 1154.35 - 844.83(1.0 + 1.7557 \times 10^{-3} f_T \mathrm{MW})^{-2.0} \quad (6)$$

$$P_C = 559.93\left(\frac{\mathrm{MW}}{f_p}\right)^{-0.638} - 1.49 \quad (7)$$

$$m = 0.4707 + 2.4831(f_m \mathrm{MW}) - \left(\frac{39.933}{f_m \mathrm{MW}}\right) \quad (8)$$

The m parameter is related to ω [2] as follows:

$$m = 0.37464 + 1.54226\omega - 0.26992\omega^2 \quad \text{for } \omega < 0.3984 \quad (9)$$

$$m = 0.379642 + 1.48503\omega - 0.164423\omega^2 + 0.016666\omega^3 \quad \text{for } \omega \geq 0.3984. \quad (10)$$

Eqs. (6)–(8) reduce to the original correlations of Kumar and Okuno [30] for n-alkanes when the perturbation parameters are 1.0. These correlations were developed using T_C, P_C, and m optimized for n-alkanes from C_7 to C_{100} in terms of the vapor pressure and liquid density using the PR EOS without volume shift. These correlations yield 3.0% and 3.4% AAD for density and vapor pressure predictions, respectively.

Use of the correlations of Kumar and Okuno [30] with the PR EOS satisfies Pitzer's definition of ω for each n-alkane. That is, the vapor pressure (P_{VAPI}) calculated at $0.7T_C$ using the PR EOS with T_C, P_C, and ω is equal to the vapor pressure (P_{VAPII}) from

$$(P_{\mathrm{VAP}})_{\mathrm{at}\ T_r = 0.7} = 10^{-(1+\omega)} P_C \quad (11)$$

using P_C and ω. This internal consistency of T_C, P_C, and ω was also satisfied for each pseudo component in the regression algorithm of Kumar and Okuno [3] by minimizing the ε function

$$\varepsilon = \frac{1}{n}\sum_{i=1}^{n} \mathrm{abs}(P_{\mathrm{VAPI}} - P_{\mathrm{VAPII}}) \quad (12)$$

where n is the number of pseudo components. A minimum in ε typically occurs when the m parameter for one of the pseudo components falls in a range between 0.94 and 0.96. The internal consistency is satisfied when one of the pseudo components has an m parameter value of 0.946 in the new algorithm presented later.

3.3. Attraction and covolume parameters

Eqs. (6)–(8) use a single value for each of the three perturbation parameters for all pseudo components. This uniform perturbation was successful in the previous PnA method for characterizing heavy oils. In this research, the PNA distribution of a plus fraction is characterized more mechanistically.

Yarborough [16] presented trend curves for specific gravity (SG) at 288.15 K and 1.01325 bars as a function of CN and "aromaticity". The aromaticity parameter was defined as the percentage of total carbon atoms in a molecule which are within the benzene ring. In our opinion, however, aromaticity in his presentation should be interpreted as deviation from n-alkanes. For example, naphthenes cannot be well defined using aromaticity, but their standard SG trend was shown to be much higher than that of n-alkanes. Nevertheless, the term "aromaticity", instead of deviation from n-alkane, is used for brevity in this paper. In Yarborough's presentation, CN ranged from 7 to 40, and aromaticity from 0 to 80. The standard SG trend curves for the aromaticity levels of 10 and 60 are reproduced in Fig. 7. The standard SG increases with CN and aromaticity. Although the trend curves of Yarborough are based on the standard SG, we use them here to show qualitatively how perturbation should be done in different regions of composition space.

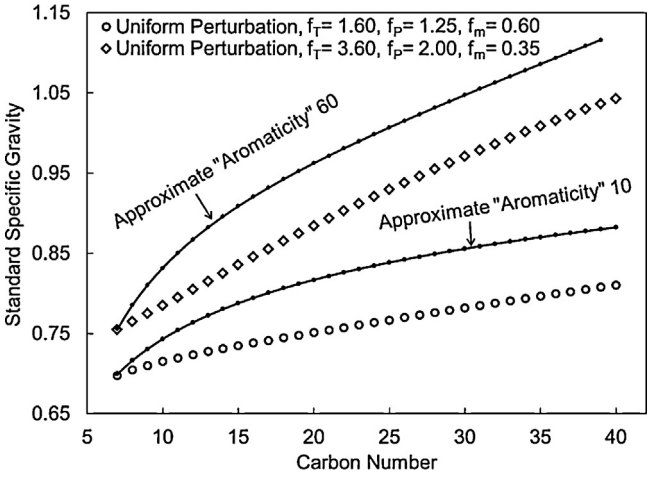

Fig. 7. Standard specific gravity (SG) calculated for aromaticity levels 10 and 60 using uniform perturbation from n-alkanes. The perturbation was made by matching the standard SG for C_7 at the two aromaticity levels given in Yarborough [16]. Critical parameters are calculated using the correlations of Kumar and Okuno [3]. The plots show that the uniform perturbation gives deviation from Yarborough's trend curves for higher CN. However, the deviation levels off at a certain CN.

Fig. 7 also shows the standard SG calculated for the aromaticity levels of 10 and 60 using the PR EOS with uniformly perturbed critical parameters. The uniform perturbations for the two aromaticity levels were conducted by matching the standard SG of C_7. Results show that the uniform perturbation gives deviation from Yarborough's trend curves for higher CN. However, the deviation levels off at a certain CN as shown in Fig. 8.

We then match the SG trend curves for CNs from 8 to 40 using variable perturbation. Fig. 9 shows the resulting

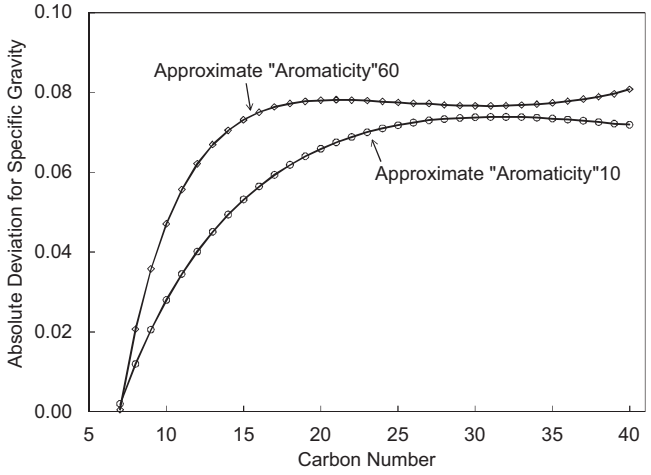

Fig. 8. Absolute deviation for standard SG calculated for two aromaticity levels 10 and 60 using uniform perturbation from n-alkanes. Absolute deviation increases with increasing carbon number and becomes nearly constant for high CNs.

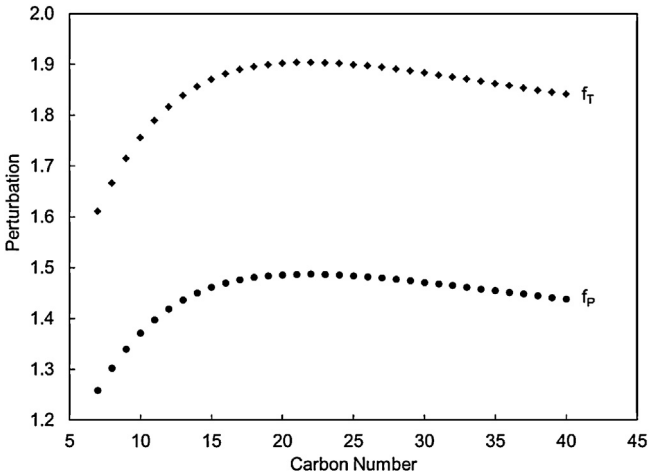

Fig. 9. Variable perturbation from *n*-alkanes to match the standard SG curves from Yarborough [16]. Aromaticity of 10 is considered. Uniform perturbation is appropriate for the higher CN range, while sharply increasing perturbation is required for the lower CN range.

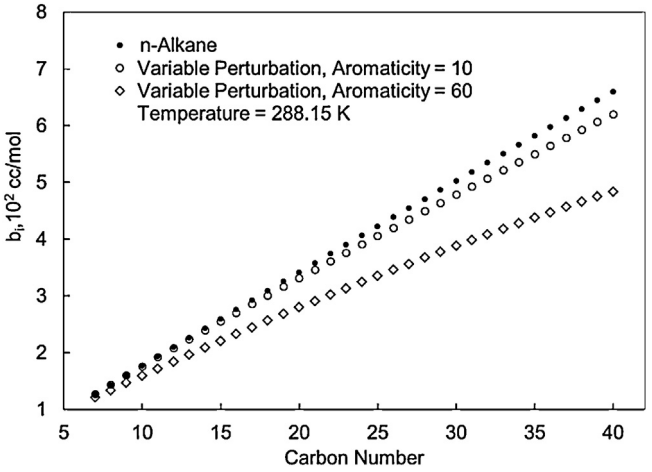

Fig. 11. The covolume (*b*) parameter for three levels of aromaticity 0, 10, and 60. The original correlations of Kumar and Okuno [30] are used for *n*-alkanes (i.e., zero aromaticity). The f_T, f_P, and f_m values fitted to Yarborough's trend curves are used for the aromaticity levels 10 and 60. Temperature is 288.15 K.

perturbation parameters for CNs from 7 to 40 for the aromaticity level of 10. Uniform perturbation is appropriate for the higher CN range, while sharply increasing perturbation is required for the lower CN range. This explains why uniform perturbation can be used for heavy-oil characterization, where CNs of all pseudo components are typically higher than 20. For lighter reservoir fluids, however, a few pseudo components usually fall in the region of composition space where perturbation should be increased with CN or MW.

Perturbations of critical parameters directly affect the attraction (*a*) and covolume (*b*) parameters of a cubic EOS, which in turn affect the Gibbs free energy and volumetric predictions in *P*–*T*–*x* space. Figs. 10 and 11 show the *a* and *b* parameters, respectively, for three levels of aromaticity 0, 10, and 60. The original correlations of Kumar and Okuno [30] are used for *n*-alkanes (i.e., zero aromaticity). The f_T, f_P, and f_m values fitted to Yarborough's trend curves are used for the aromaticity levels 10 and 60. The *a* parameter increases with CN for a fixed aromaticity level. The effect of aromaticity on the *a* parameter is not systematic, i.e., the a parameter increases with aromaticity for light hydrocarbons, and the trend is the other way around for heavier hydrocarbons. The trend of the b parameter is more systematic. The b parameter for *n*-alkane is higher than those for aromatic hydrocarbons for a given CN. Also, *n*-alkanes exhibit the largest gradient of the b parameter with respect to CN.

Fig. 12 shows a parameter group a/b^2 (ψ) based on the values for the *a* and *b* parameters in Figs. 10 and 11. The ψ parameter for each component can be calculated using the PR EOS as follows:

$$\psi = \frac{\Omega_a}{\Omega_b^2} P_C \alpha(T) \tag{13}$$

The ψ parameter is a function of T_C, P_C, ω, and T as shown in Eq. (13). The ψ parameter is sensitive to the level of aromaticity for light and intermediate hydrocarbons, where variable perturbation is required (see Fig. 12). This is also true at a realistic reservoir temperature of 370.15 K as shown in Fig. 13. We therefore use the ψ parameter to control variable perturbation in different regions of composition space.

The ψ parameter behavior with respect to CN and aromaticity depends on the functional form of the EOS used (the PR EOS in this research). The ψ parameter monotonically decreases with CN for high aromaticity levels, but exhibits a maximum for low aromaticity levels including *n*-alkanes. The ψ parameter for a fixed CN increases with increasing level of aromaticity, and changes its

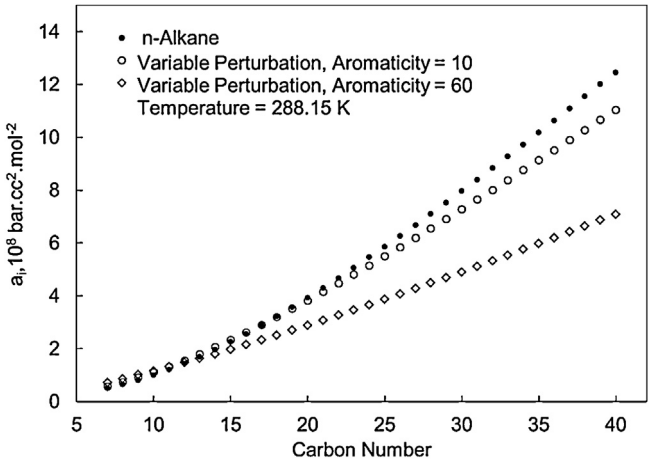

Fig. 10. The attraction (*a*) parameter for three levels of aromaticity 0, 10, and 60. The original correlations of Kumar and Okuno [30] are used for *n*-alkanes (i.e., zero aromaticity). The f_T, f_P, and f_m values fitted to Yarborough's trend curves are used for the aromaticity levels 10 and 60. Temperature is 288.15 K.

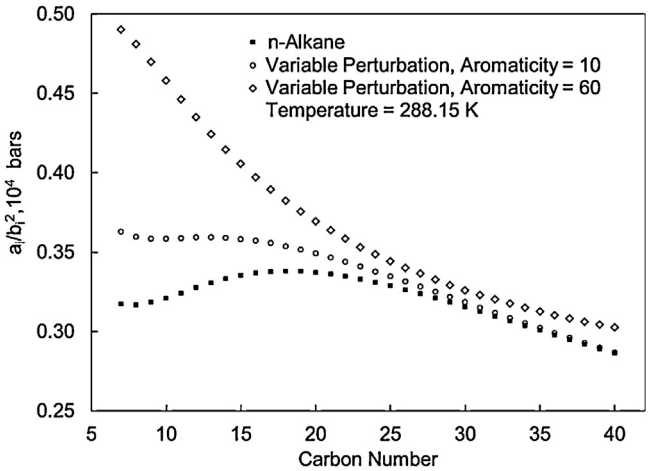

Fig. 12. The ψ parameter ($\psi = a/b^2$) for three levels of aromaticity based on the values for the *a* and *b* parameters in Figs. 10 and 11. Temperature is 288.15 K. The ψ parameter for each component is calculated using Eq. (13).

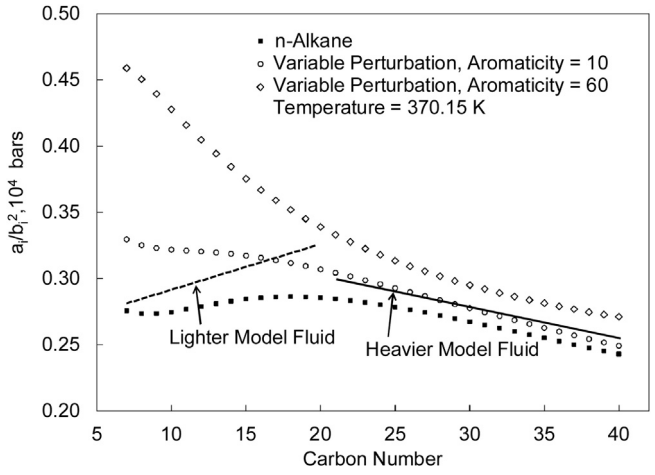

Fig. 13. The ψ parameter ($\psi = a/b^2$) for three levels of aromaticity at 370.15 K. All critical parameters and acentric factors are the same as those used in Figs. 10 and 11. The ψ parameter changes its sensitivity to aromaticity around the CN of 20. Trend curves are given for the lighter and heavier model fluids. For the model trends, the physical trend is also considered that heavier fractions are relatively more naphthenic and aromatic than lighter fractions.

sensitivity to aromaticity around CN 20 as shown in Figs. 12 and 13 at different temperatures.

Van Konynenburg and Scott [35] used the ψ parameter in their pioneering research on classification of binary phase diagrams using the van der Waals EOS. The ψ parameters for two components (i.e., ψ_i, where $i = 1, 2$) were used to characterize size-asymmetric binary mixtures.

Fig. 13 is useful in considering qualitatively how the ψ parameter should be characterized depending on the fluid composition of interest. In general, heavier fractions are relatively more naphthenic and aromatic than lighter fractions [16,36]. This physical trend is plausible considering that a larger number of carbon atoms allow for more variations of hydrocarbon molecular structures; e.g., if the uniform distribution of molecular structures is considered within individual CN groups, the concentration of *n*-alkane becomes lower for higher CN.

Let us consider two model fluids; the lighter and heavier model fluids. The lighter model fluid has all pseudo components within the range of C_7–C_{20}. The heavier model fluid has all pseudo components heavier than C_{20}. The lighter model fluid has a CN range for pseudo components that is much narrower than the heavier model fluid as can be expected from Fig. 6. In the CN range higher than approximately 20, the ψ parameter decreases with CN for a given level of aromaticity, and is insensitive to the level of aromaticity. Therefore, the decreasing ψ trend with respect to CN is considered for the heavier model fluid in Fig. 13. In the CN range lower than approximately 20, the ψ parameter is sensitive to the level of aromaticity within the narrow CN range. Therefore, the increasing ψ trend with respect to CN is considered for the lighter model fluid in Fig. 13.

The ψ parameter typically increases with CN (like the lighter model fluid in Fig. 13), if all pseudo components are within the range of C_7–C_{20}. For some heavy oils, the lightest pseudo component can be around C_{20}, and the ψ parameter is expected to decrease almost linearly with CN (like the heavier model fluid in Fig. 13). For many fluids, however, the CN range of pseudo components contains the boundary of the two distinct regions, which is approximately C_{20}. For these fluids, the ψ parameter exhibits combinations of these two model trends depending on the CN range of their pseudo components and their average aromaticity. The two model trends in Fig. 13 are shown to be linear for simplicity. Actual trends of characterized fluids are non-linear in general as shown in the next section.

We assume use of four pseudo components based on the Chi-squared compositional characterization for discussion here. CN ranges observed for various fluids in our research can be summarized as follows: 7–30 for gas condensates, 9–45 for light oils, 11–60 for intermediate oils, and 13–85 for heavy oils. Light gas condensates, for which the C_{7+} fraction is less than 2%, can have all four pseudo components within the CN range from 7 to 20. Their ψ trends can be strongly influenced by the *n*-alkane curve, which exhibits a convex trend (see Fig. 13).

The overall composition information can be obtained by the distribution function fitted to the composition data available. The PnA method considers an expected trend of ψ in the regression process depending on the p parameter value obtained from the fitted Chi-squared distribution. Uniform perturbation is suitable for heavy oils as presented in Kumar and Okuno [3]. This can be also seen in Fig. 9, which shows that uniform perturbation is appropriate for heavier fractions using the PR EOS. Hence, the p parameter value of 10 corresponding to extra heavy oils is considered as the limiting value, for which perturbation is uniform. With increasing API gravity, the p parameter value decreases below 10, and variable perturbation is required according to the ψ trends discussed above.

3.4. Regression algorithm

In this subsection, we discuss briefly how the current PnA method implements the new concept regarding the ψ parameter presented in the previous subsection. The main difference from the regression algorithm of Kumar and Okuno [3] is that the perturbation parameters f_T, f_P, and f_m in Eqs. (6)–(8) are augmented by a fourth adjustment parameter γ. We measure a deviation of the fluid of interest from the limiting fluid with the p parameter value of 10 using constants d_j, where j is the component index for pseudo components. The d constants are calculated specifically to a given fluid, and collectively serve as a fluid type indicator. Then, the d constants and the fourth adjustment parameter γ are combined to have a desired trend of the ψ parameter, considering the overall composition of a fluid and CNs of pseudo components within that fluid.

The algorithm uses four adjustment parameters f_T, f_P, f_m, and γ to match the saturation pressure at the reservoir temperature and liquid densities at different pressures and the reservoir temperature. Volume shift parameters are not used in the PnA method. BIPs are constant as described in Kumar and Okuno [3]. The BIPs used in the PnA method are 0.0 for N_2-CO_2, 0.1 for N_2-C_i, where $1 \le i \le 6$, 0.13 for N_2-pseudo-components, and 0.1 for CO_2-hydrocarbons. BIPs are zero for hydrocarbon–hydrocarbon pairs. The algorithm is presented below in a step-wise manner, and in Appendix A using a flow chart.

Step 1. Composition characterization: Using the composition data available, the plus fraction is split into n pseudo components using the Chi-squared distribution function (Eq. (5); see Quiñones-Cisneros et al. [34]). This step gives the mole fractions and MWs of n pseudo components and the p value of the fluid.

Step 2. Calculation of gradation constants d_j: The mole fractions and MWs of n pseudo components are calculated assuming that the fluid p value is 10. We calculate the ratios of the MWs from step 1 to the MWs with the assumption of p equal to 10. The resulting ratios are normalized with respect to the ratio for the lightest pseudo component. These normalized ratios are the d_j constants, where $j = 1, 2, \ldots, n$. That is, d_1 is always 1.0.

Step 3. Check for the necessity of using density data. Characterize the fluid assuming that f_T, f_P, and f_m are equal to 1.0 in Eqs. (6)–(8). Compare density calculations using the PR EOS to the experimental

density data. If the average density deviation indicates overprediction of the densities, than go to step 5. Otherwise, continue to step 4 below.

Step 4. Characterization using density and saturation pressure data.

i. $f_T = 1.0$, $f_P = 1.0$, $\gamma = 0.0$, and $k = 1$, where k is the iteration index.

ii. Find f_m with which T_C, P_C, and m are internally consistent using

$$m_j = 0.4707 + 2.4831\left(f_{mk}\mathrm{MW}_j d_j^{\gamma k}\right)^{-(39.933/(f_{mk}\mathrm{MW}_j d_j^{\gamma k}))} \quad (14)$$

In each iteration, f_m is adjusted until one of the pseudo components has an m parameter value equal to 0.946.

iii. Calculate critical parameters using

$$T_{cjk} = 1154.35 - 844.83(1.0 + 1.7557 \times 10^{-3} f_{Tk} d_j^{\gamma k}\mathrm{MW}_j)^{-2.0} \quad (15)$$

$$P_{cjk} = 559.93\left(\frac{\mathrm{MW}_j}{f_{Pk} d_j^{\gamma_k}}\right)^{-0.638} - 1.49 \quad (16)$$

iv. Adjust f_T and f_P to match the saturation pressure and density data.

v. Update γ using

$$\gamma_k = 0.5[\gamma_{k-1} + z_1(3.464 + h)f_{\mathrm{avg}}], \quad (17)$$

where $f_{\mathrm{avg}} = (f_{T,k-1}^{2\theta} + f_{P,k-1}^{2\theta} + f_{m,k-1}^{2\theta})/(f_{T,k-1} + f_{P,k-1} + f_{m,k-1})$. $\theta = (3.0 + h)h$, h is the harmonic mean of z_L, z_I, and z_H; z_L: mole fraction of methane in the overall composition; z_I: sum of the mole fractions of N_2, CO_2, and C_i, where $i = 2, 3, \ldots, 6$. z_H: mole fraction of C_{7+}. f_T and f_P are set to 1.0, and go to step 4-ii until the difference of the γ values between two consecutive iterations becomes below a tolerance; e.g., 10^{-3}.

Step 5. Characterization using only saturation pressure data.

$f_T = 0.97$, $f_P = 0.97$, $\gamma = 0.0$ (for bubble point search), $\gamma = 1.5$ (for dew point search), and $k = 1$, where k is the iteration index.

Find f_m with which T_C, P_C, and m are internally consistent using Eq. (14).

Calculate critical parameters using Eqs. (15) and (16).

Adjust γ until the saturation pressure is matched.

The maximum overprediction in step 3 that we observed in this research is 4%, which is quite accurate. Such accurate density prediction in step 3 indicates that phase behavior of the fluid is similar to that of a n-alkane mixture using the PR EOS. We observed in this research that density matching is not needed for such fluids because of the small density errors.

Eqs. (14)–(16) are based on our correlations presented in [30], but also consider the four adjustment parameters (f_T, f_P, f_m, and γ) and the d constants. Eqs. (14)–(16) reduce to the original forms developed for n-alkanes in [30] when $f_T = f_P = f_m = 1.0$ and $\gamma = 0.0$.

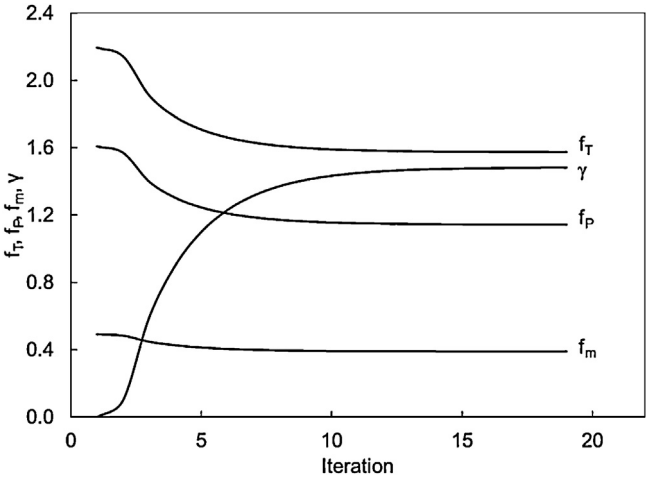

Fig. 14. Trends of the f_T, f_P, f_m, and γ parameters during iteration for oil 2 given in Table 2. As γ increases from the starting value of zero, f_T, f_P, and f_m decrease. Convergence is achieved when the rate of increase in γ or the rate of decrease in f_T, f_P, and f_m becomes negligible.

Eq. (17) was designed to achieve a qualitative trend that the converged γ value decreases as the fluid becomes heavier. Obviously, there are many other possibilities for the iteration scheme that achieves this qualitative trend. Eq. (17) is a successful model that we developed in this research. z_I, h, and f_{avg} in Eq. (17) decreases for heavier fluids in general. The main consideration points in the model development include the following:

- $0 < h \leq 1/3$, and the equality holds for the uniform distribution of components
- z_I typically decreases for heavier fluids
- h typically decreases for heavier fluids
- θ decreases as h decreases (note that $h > 0$)
- f_{avg} becomes the self-weighted average when θ is unity, or when the component distribution is not very skewed with h of 0.3028. f_{avg} typically decreases for heavier fluids. This is because for heavier fluids, f_T and f_P typically increases above 1.0, and f_m typically decreases below 1.0.

Fig. 14 shows an example trend of the four adjustment parameters f_T, f_P, f_m, and γ during iteration when oil 2 (39.89°API) in Table 2 is characterized using the above algorithm. As γ increases from the starting value of zero, f_T, f_P, and f_m decrease. Convergence is achieved when the rate of increase in γ or the rate of decrease in f_T, f_P, and f_m becomes negligible. The internal consistency of T_C, P_C, and m is evaluated by the ε function given in Eq. (12). Fig. 15 shows

Table 2
Converged f_T, f_P, f_m, p, and γ values for reservoir oils characterized using the PnA method. Slim-tube MMPs are reported for these oils in the literature.

Oil No.	References	MW (g/mol)	°API	Res. temp. (K)	No. of density data	f_T	f_P	f_m	p	γ
1	[37], F1	135.24	35.22[a]	374.85	5	1.091	1.101	0.399	4.5	1.236
2	[37], F2	136.25	39.89	372.05	6	1.574	1.143	0.389	4.7	1.481
3	[37], F3	82.41	39.31[a]	387.35	11	1.239	1.026	0.500	6.3	0.977
4	[37], F4	63.17	40.34[a]	388.20	7	0.959	0.959	0.545	3.0	0.770
5	[37], F5	125.82	32.04[a]	394.25	12	1.347	1.124	0.412	4.5	1.318
6	[37], F6	96.25	37.73[a]	373.15	5	1.072	1.060	0.488	4.2	1.067
7	[37], F7	96.19	41.06[a]	393.15	12	1.357	1.060	0.443	4.9	1.383
8	[37], F11	82.55	38.71[a]	373.75	11	1.172	1.066	0.501	3.8	0.921
9	[37], F13	150.2	35.64[a]	377.55	8	1.499	1.038	0.319	4.4	0.996
10	[55], F1	161.42	31.85	350.40	16	1.538	1.196	0.347	4.6	1.341
11	[55], F2	109.37	40.03	353.70	17	1.418	1.086	0.392	3.9	1.304

[a] As reported. All other API gravities are calculated from density at 288.15 K and 1.01325 bars.

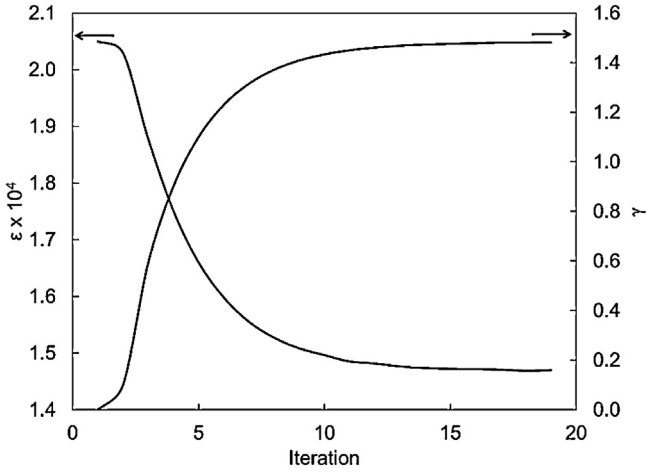

Fig. 15. Trends of the ε function and the γ parameter during iteration for oil 2 given in Table 2. The ε function is defined in Eq. (12). In our earlier work (Kumar and Okuno [3]), the ε function was the stopping criterion in regression. Here, the ε function is not the stopping criterion in regression. The ε function decreases with increasing γ value, and is sufficiently small on convergence.

that the ε function decreases with increasing γ and is sufficiently small on convergence. The algorithm is written in FORTRAN, and takes less than two minutes on average per fluid using the Intel Core i7-960 processor at 3.20 GHz and 8.0 GB RAM.

Gas condensates and light volatile oils behave like *n*-alkane mixtures due to low concentrations of the C_{7+} fraction. For these fluids, density data are not required in the PnA method. The next section shows that the correlations of Kumar and Okuno [30] enable the PR EOS to accurately predict densities in such cases.

The key parameter in the PnA method is γ, which controls the ψ gradient with respect to CN (or MW) of pseudo components. Hence, adjustment of γ can be carried out using more data, instead of using Eq. (17). For example, liquid saturation data from constant volume depletion (CVD) and constant composition expansion (CCE), slim-tube MMPs, and three-phase data can be used to adjust γ. For solubility data, BIPs may be adjusted for methane and heavier pseudo components to change phase behavior predictions locally in composition space. As is shown in the next section, the PnA method systematically and monotonically adjusts phase behavior predictions using a few adjustment parameters, unlike the conventional methods.

The PnA method preserves physical trends of parameters by (1) starting with the values optimized for a homologous series of *n*-alkanes, (2) limiting the number of adjustment parameters, and (3) perturbation based on physical considerations described in sections 1, 3.2, and 3.3. Pedersen and Christensen [5] recommended using coefficients in their T_C, P_C, and m correlations [45,46] as regression parameters, instead of individual components' T_C, P_C, and m (or ω). With this approach, it is easier to maintain smooth variations of T_C, P_C, and m with respect to CN. However, physical trends are achieved only when appropriate limits are considered for the coefficient values. This approach gives 13 coefficients as possible regression parameters, apart from volume-shift parameters. The number of regression parameters actually used is restricted to keep the number of regression parameters smaller than the number of data points. Selection of regression parameters is made based on the sensitivity to the difference between phase behavior predictions and data points in Pedersen and Christensen [5].

4. Application of the PnA method

In this section, the PnA method is applied to 77 reservoir fluids, ranging from 9.5°API to 71.1°API, where 12 components are used altogether; N_2, CO_2, C_1, C_2, C_3, C_4, C_5, C_6, and four pseudo components. Data available and used for characterization are (i) overall compositions, (ii) saturation pressures at reservoir temperatures, and (iii) liquid densities at different pressures at reservoir temperatures, unless otherwise stated. Other types of data available, such as MMPs, CVD, and CCE, are not used in characterization, but are used to evaluate the reliability of characterized fluid models.

The significance of considering the ψ parameter is first presented using oils listed in Table 2. Predictions from the PR EOS with the PnA characterization are then compared with data for various fluids in Section 4.2.

4.1. Significance of the ψ parameter

In the previous section, we discussed that perturbation from *n*-alkanes should consider the CN range of the pseudo components used. Uniform perturbation is appropriate for heavy oils since all pseudo components usually fall in the higher CN range where the ψ parameter is insensitive to the level of aromaticity. For lighter fluids, some of pseudo components are in the lower CN range where the ψ parameter is sensitive to the level of aromaticity (see Fig. 13). Variable perturbation should be considered to obtain appropriate trends of the ψ parameter for these fluids.

The ψ parameter for the PR EOS is a function of T_C, P_C, and m at a given temperature as shown in Eq. (13). Obviously, different characterization schemes result in different trends of the ψ parameter. To see this, oil 1 (35.22°API) in Table 2 is characterized using four different schemes;

Case 1. The PnA method with uniform perturbation (i.e., γ is fixed at zero)
Case 2. The PnA method with variable perturbation (i.e., the algorithm presented in the previous section)
Case 3. The conventional method using the PVTsim software without volume shift ($CM_{w/o}V$)
Case 4. The conventional method using the PVTsim software with volume shift (CM_wV).

Case 1 corresponds to the previous PnA method presented in Kumar and Okuno [3]. Cases 3 and 4 are based on step-wise manual adjustment of T_C, P_C, and ω as described in detail in Kumar and Okuno [3]. The number of components used is 12 for all cases. The CMs use the default BIP values from PVTsim as they would be the most suitable values for PVTsim. They are −0.017 for N_2-CO_2, 0.0311 for N_2-C_1, 0.0515 for N_2-C_2, 0.0852 for N_2-C_3, 0.08 for N_2-C_4, 0.1 for N_2-C_5, 0.08 for N_2-C_i, where $i \geq 6$, 0.12 for CO_2-C_j, where $1 \leq j \leq 6$, and 0.1 for CO_2-pseudo-components. As in the PnA method, BIPs are zeros for hydrocarbon-hydrocarbon pairs in the CMs. For a fair comparison, the same composition characterization based on the Chi-squired distribution is used for the four cases. Saturation pressure and density data are matched by adjusting T_C, P_C, and ω for cases 1–3. For case 4, saturation pressure is matched using T_C, P_C, and ω. The change of T_C, P_C, and ω also alters density predictions, but they are not necessarily accurate yet. Then, only volume shift parameters are used to match density data. We calculate the MMPs for the oil with injection gas (0.48% N_2, 4.97% CO_2, 58.22% C_1, 17.14% C_2, 12.10% C_3, 4.97% C_4, 1.66% C_5, and 0.53% C_6) at the reservoir temperature 374.85 K. The corresponding slim-tube MMP is reported to be 220 bars in Jaubert et al. [37].

The resulting trend of ψ along with the AD on the MMP is shown for each case in Fig. 16. The CN range of the pseudo components is approximately from 11 to 40, which is similar to the entire CN range presented in Fig. 13. Case 1 with uniform perturbation exhibits a monotonically decreasing trend of ψ with respect to CN for the four pseudo components. The calculated MMP has a large AD of +19% compared to the slim-tube MMP. Considering the

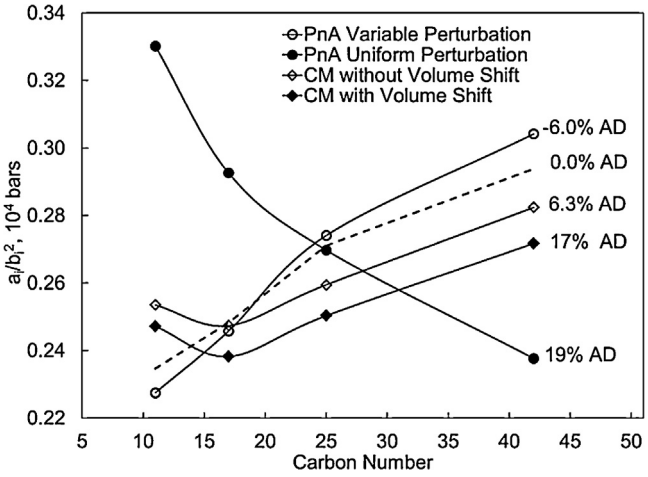

Fig. 16. The ψ parameter ($\psi = a/b^2$) for oil 1 given in Table 2. Four different schemes are used for characterization; PnA with uniform perturbation, PnA with variable perturbation, $CM_{w/o}V$, and CM_wV. The dashed curve shows the ψ trend when the PnA method uses γ of 1.08 to match the slim-tube MMP of 220 bars.

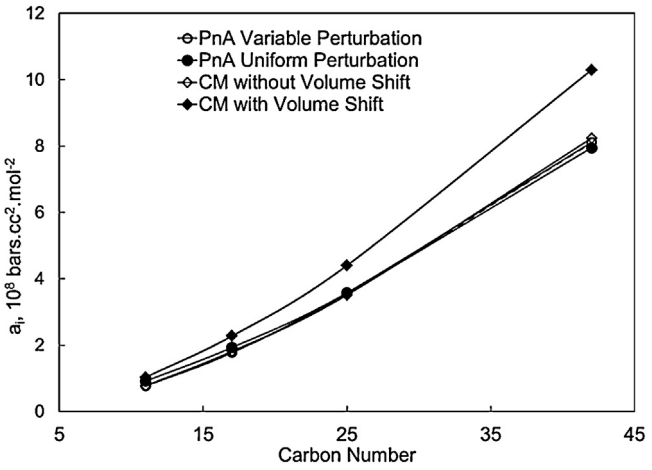

Fig. 18. The trend of the a parameter for the four pseudo components for each of four cases considered in Fig. 16 The dashed curve shows the trend for the a parameter when the PnA method uses γ of 1.08 to match the slim-tube MMP of 220 bars.

approximate CN of 11 for the lightest pseudo component, the negative slope of ψ is not expected. Cases 3 and 4 present an obvious minimum in the trend of ψ with respect to CN. Even though the MMP calculated for case 3 is relatively accurate, it may be difficult to justify such ψ trends, considering the CN range of the pseudo components and that heavier pseudo components are more naphthenic and aromatic than lighter pseudo components in general [16]. Use of volume shift in case 4 makes the calculated MMP less accurate due to the fundamental reasons presented in the section on Effect of Volume-Shift Parameter Regression on Gibbs Free Energy. Case 2 shows a monotonically increasing trend of ψ with respect to CN. The converged γ is 1.23. Considering the inevitable dispersion effects in slim-tube tests, the AD of −6.0% is acceptable in this case.

Matching MMP data in fluid characterization has been proposed in the literature (e.g., Egwuenu et al. [38]). It will be easy to implement this proposal in the PnA method. Fig. 17 shows the MMPs calculated for different γ values. A monotonic change in the calculated MMP is observed with respect to γ. The slim-tube MMP of 220 bars can be predicted with γ of 1.08, and the corresponding ψ trend is shown by a dashed line in Fig. 16. Although matching a slim-tube MMP without considering dispersion effects has little practical importance, this exercise shows that phase behavior predictions can be adjusted systematically and monotonically with the PnA method. Similar control over phase behavior predictions is difficult with the CM.

Figs. 18 and 19 show the *a* and *b* parameters for the four pseudo components for each of the four cases. The dashed curves correspond to the case for γ of 1.08. Case 4 deviates significantly from the other cases in the *a* and *b* parameters. However, it is case 1 that has the largest error in the MMP calculation as shown in Fig. 16. The *a* and *b* parameters are interdependent in fluid characterization, and the ψ parameter properly captures the interrelationship between the *a* and *b* parameters. Cases 1–3 are similar in the trends of the *a* and *b* parameters. However, the ψ parameter effectively makes the differences among the cases more marked.

For all oils in Table 2, slim-tube tests and measured MMPs are reported in the literature. Table 3 lists slim-tube and calculated MMPs for eight oils from Table 2, one of which is oil 1 discussed above. A small amount of C_{7+} contained in some of the injection gases is discarded for the MMP calculations (their C_{7+} concentrations are less than 0.3%). Two cases are considered for these MMP calculations; one with variable perturbation and the other with uniform perturbation. The AAD on the MMP calculations is 6.7% for

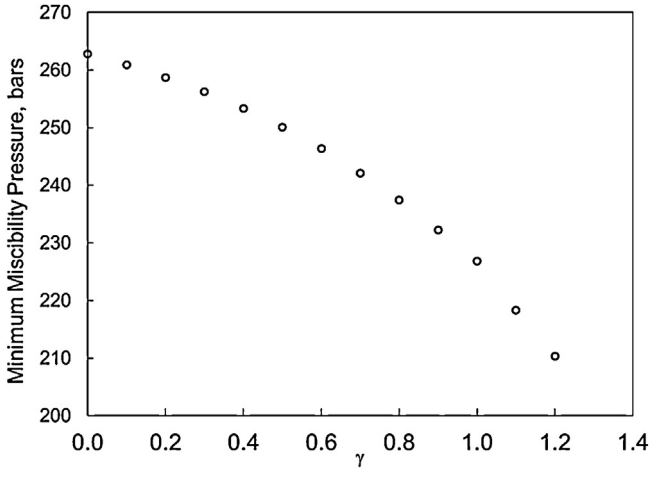

Fig. 17. Minimum miscibility pressures calculated for different γ values for oil 1 (Table 2) with injection gas (0.48% N_2, 4.97% CO_2, 58.22% C_1, 17.14% C_2, 12.10% C_3, 4.97% C_4, 1.66% C_5, and 0.53% C_6) at 374.85 K. A monotonic change in the calculated MMP is observed with respect to γ. The slim-tube MMP of 220 bars can be predicted with γ of 1.08.

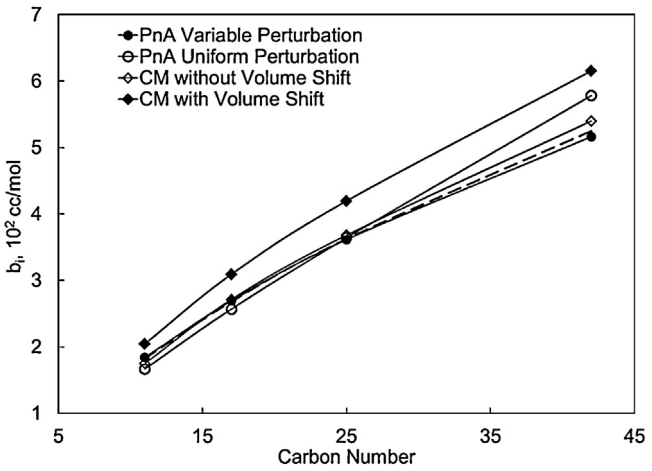

Fig. 19. The trend of the *b* parameter for the four pseudo components for each of four cases considered in Fig. 16 The dashed curve shows the trend for the b parameter when the PnA method uses γ of 1.08 to match the slim-tube MMP of 220 bars.

Table 3
Slim-tube and calculated MMPs for eight oils from Table 2.

Oil No. (From Table 2)	°API	Slim-tube MMP, bars	Variable perturbation PnA method, MMP (bars)	Uniform perturbation PnA method ($\gamma = 0$), MMP (bars)
1	35.22	220	207.86	262.00
2	39.89	220	258.79	339.00
3	39.31	376	366.84	446.52
4	40.34	379	350.61	437.56
5	32.04	366	341.00	496.12
6	37.73	309	296.16	371.33
7	41.06	296	317.00	357.50
8	38.71	335	343.00	435.03
AAD%			6.70	26.70

the former case and 26.7% for the latter case. These results further indicate the significance of considering the ψ parameter in perturbation using γ. The AAD from the new PnA method is similar to the result of Jaubert et al. [39], who conducted MMP calculations for the same oils. Unlike the PnA method, they developed fluid models using various data from standard *PVT* measurements, swelling tests, and multicontact tests.

4.2. Case studies

The 77 different fluids considered here are 34 heavy and black oils, 12 volatile oils (including one near-critical fluid), and 31 gas condensates (including three near-critical fluid). These fluids are listed in Table 2 and Tables 4–6.

For oils 1–22 listed in Table 4, available data are limited to overall compositions, saturation pressures, and liquid densities that are used in characterization. Most of them are heavy oils, for which data are in general scarce in literature [40,41]. Therefore, pseudo data [42] are generated for MMPs with pure CO_2 and pure C_1 and some three-phase envelopes using 30 components based on the $CM_{w/o}V$ [5,26,43–47] as explained in detail in Kumar and Okuno [3]. The 30 components consists of N_2, CO_2, C_1, C_2, C_3, C_4, C_5, C_6, and 22 pseudo components for the C_{7+} fraction. We have used the default BIP values in PVTsim [48] for $CM_{w/o}V$ as presented in the previous subsection. Using the $CM_{w/o}V$, the effects of the number of components on phase behavior predictions diminish when more than 16 components are used [3]. Thus, use of 22 pseudo components is appropriate to avoid errors caused by reduction of composition space. We directly use the compositions characterized by Quiñones-Cisneros et al. [34] for oils 1–13, 18, and 22 in Table 4.

Tables 5 and 6 list volatile oils and gas condensates, respectively, for which *PVT* data are available, such as CVD and CCE data. MMP data are unavailable for the volatile oils.

Tables 2, 4 and 5, and 6 present converged γ values and corresponding f_T, f_P and f_m values, which are plotted with respect to the API gravity in Figs. 20–23. The converged f_T and f_P values are greater than 1.0, and the converged f_m values are smaller than 1.0. The overall trends indicate that heavier fluids tend to require more perturbation from *n*-alkanes. This is consistent with the physical trend that heavier fractions are relatively more naphthenic and aromatic than lighter fractions [16,36].

The γ parameter plays an important role in the extended PnA method. It controls the gradient of ψ with respect to MW or CN for pseudo components. Fig. 23 shows that the γ parameter becomes greater for lighter fluids. This is because a lighter fluid contains pseudo components lighter than C_{20} at higher concentrations. The ψ parameter is sensitive to aromaticity for such lower CNs as shown in Fig. 13. For heavy oils, variable perturbation from *n*-alkanes is less significant; the importance of the ψ and γ parameters diminishes as the API gravity becomes lower as shown in Fig. 23. For extra heavy oils, the PnA method reduces to the previous PnA method developed in Kumar and Okuno [3].

Table 4
Converged f_T, f_P, f_m, p, and γ values for reservoir oils characterized using the PnA method. For these oils, available data are limited to overall compositions, saturation pressures, and liquid densities.

Oil No.	References	MW (g/mol)	°API	Res. temp. (K)	No. of density data	f_T	f_P	f_m	p	γ
1	[56], Oil-8	443.08	9.50	322.05	13	2.064	1.728	0.361	8.0	0.091
2	[56], Oil-7	431.59	11.63	322.05	12	1.683	1.647	0.370	8.0	0.041
3	[33], Oil-6	377.88	13.38	322.05	13	2.871	1.819	0.245	7.5	0.063
4	[33], Oil-5	422.94	11.98	322.05	13	1.787	1.659	0.381	7.5	0.048
5	[33], Oil-1	170.59	20.81	330.40	16	2.879	1.760	0.403	6.0	0.084
6	[34], Oil-8	182.05	24.25	333.15	16	2.771	1.893	0.429	9.0	0.227
7	[34], Oil-7	159.99	29.24	330.40	16	2.288	1.731	0.439	8.0	0.088
8	[34], Oil-6	118.18	35.61	346.15	5	1.802	1.514	0.414	7.0	1.092
9	[34], Oil-5	130.55	28.30	337.85	3	2.781	1.786	0.444	6.0	0.200
10	[34], Oil-4	114.57	33.35	337.85	6	2.248	1.600	0.468	5.5	0.443
11	[34], Oil-3	87.80	40.46	337.25	5	1.744	1.256	0.470	4.0	0.988
12	[34], Oil-2	89.83	47.63	366.45	11	1.419	1.047	0.446	4.0	0.809
13	[34], Oil-1	86.57	60.18	427.60	13	1.128	1.000	0.585	2.5	0.340
14	Oil[a]	296.90	22.60[b]	357.50	13	1.936	1.433	0.284	5.7	0.535
15	[57], Oil-1	123.79	34.04	355.37	8	2.249	1.646	0.394	6.6	1.011
16	[57], Oil-6	83.31	40.90[b]	385.37	20	1.325	1.033	0.440	4.1	1.390
17	[57], Oil-7	113.60	39.70[b]	328.15	20	1.334	0.997	0.390	3.7	1.459
18	[58], Oil-5	240.24	20.19	345.93	15	2.615	1.815	0.343	4.0	0.110
19	[59], Light Oil	105.28	43.68	377.59	8	1.075	0.978	0.436	6.1	1.309
20	[46], Fluid-1	124.57	35.73	344.75	8	2.160	1.532	0.462	5.8	0.402
21	[57], Oil-4	96.22	41.30[b]	316.48	10	1.546	1.152	0.423	4.6	1.498
22	[56], L-Oil-2	80.90	62.40	418.15	22	1.402	1.033	0.446	2.5	1.312
23	[60], West Sak Oil	228.88	18.68	299.81	10	1.635	1.605	0.566	5.7	0.048

[a] This is an actual oil, but the source is not mentioned for confidentiality.
[b] As reported. All other API gravities are calculated from density at 288.15 K and 1.01325 bars.

Table 5
Converged f_T, f_P, f_m, p, and γ values for volatile oils characterized using the PnA method. *PVT* data are available for these oils, such as CVD and CCE data.

Oil No.	References	MW (g/mol)	°API	Res. temp. (K)	f_T	f_p	f_m	p	γ	Data limits value (type[b])	Dev.[c]
1	[61], Fluid-12	46.07	50.3	354.82	1.018	1.018	0.562	2.3	0.620	38.20 (1)	3.19
2	[61], Fluid-13	56.06	36.7	364.82	1.972	1.344	0.437	2.3	0.503	3.93 (3)	0.02
3	[61], Fluid-14	54.57	40.7	360.93	1.412	1.188	0.486	2.4	0.555	1.00 (3)	0.01
4	[61], Fluid-15	51.11	57.5	353.15	1.106	0.973	0.662	2.9	0.829	2.98 (3)	0.02
5	[61], Fluid-16	59.63	55.6	425.93	0.957	0.957	0.525	2.5	0.600	35.30 (1)	2.12
6	[61], Fluid-17	67.32	44.5	414.82	1.179	0.998	0.418	2.5	0.806	6.84 (3)	0.03
7	[61], Fluid-18	59.90	54.4	423.15	0.980	0.991	0.628	3.2	0.569	7.57 (3)	0.03
8	[61], Fluid-19	62.65	59.5	377.59	1.092	0.977	0.458	4.3	1.315	4.06 (3)	0.01
9	Oil[e]	86.68	56.6	376.75	1.568	1.048	0.487	4.0	1.144	2.46 (3)	0.01
10	[62], Oil A	50.93	44.5[a]	408.70	0.956	0.956	0.643	2.5	0.670	33.30 (1)	6.38
11	[62], Oil B	57.50	56.7	393.70	0.956	0.956	0.596	3.1	0.760	49.50 (1)	3.13
12	[63][d]	37.94	57.5	371.60	1.043	1.043	0.648	2.0	0.280	13.69 (2)	2.93

[a] As reported. All other API gravities are calculated from density at 288.15 K and 1.01325 bars.
[b] (1) is CVD liquid saturation (%), (2) is CCE liquid saturation (%), (3) is CCE relative volume (v/v).
[c] Deviation = sum of absolute of (experimental value – predicted value)/number of data point.
[d] Oil No. 12 is near critical.
[e] This is an actual oil, but the source is not mentioned for confidentiality.

Fig. 24 depicts the average gradient of ψ with respect to MW of pseudo components ($\Delta\psi/\Delta M$). This average gradient is calculated using ψ's and MWs for the lightest and heaviest pseudo components. The gradient is small for heavy fluids, and gradually increases as the API gravity increases. This is consistent with the trends of ψ for the two model fluids presented in Fig. 13. Fig. 25 shows the variation of the ψ gradient with respect to γ. As γ increases, the gradient also increases. These figures indicate that the algorithm successfully converged as designed in the previous section. The ψ parameter is effectively controlled by adjusting γ.

4.2.1. MMP calculations

We showed that the extended PnA method gives better MMP predictions than the previous PnA method for eight oils in Table 2. Here, we further test the extended PnA method for oils 1–22 in Table 4. MMPs at reservoir temperatures are calculated for 100% C_1 using PVTsim [48] and for 100% CO_2 using PennPVT [49,50]. CO_2-MMP for oils 1, 2, 4, and 18 in Table 4 are not considered because of the presence of three phases during the MMP calculations.

Figs. 26 and 27 compare the MMPs from the PnA method and those from pseudo data. Good agreement is observed between them for heavy oils and light oils. Some oils in the range of

Table 6
Converged f_T, f_P, f_m, p, and γ values for gas condensates characterized using the PnA method. *PVT* data are available for these oils, such as CVD and CCE data.

Fluid No.	References	MW (g/mol)	°API	Res. temp. (K)	f_T and f_p	f_m	p	γ	Maximum data value (Type[b])	Dev.[c]
1	[61], Fluid-3	31.53	58.3	424.82	0.972	0.485	2.0	0.760	11.70 (1)	1.15
2	[61], Fluid-4	31.44	59.9	403.15	0.970	0.513	2.0	0.680	13.00 (1)	2.12
3	[61], Fluid-5	32.41	60.4	382.59	0.974	0.530	2.1	0.730	23.30 (2)	5.54
4	[61], Fluid-7	36.62	59.6	397.59	0.975	0.756	2.6	0.720	25.00 (1)	5.38
5	[61], Fluid-8	40.77	62.9	424.82	0.970	0.710	2.2	0.410	30.40 (1)	1.63
6[d]	[61], Fluid-10	39.23	64.7	422.59	0.971	0.545	3.3	0.670	33.60 (1)	1.15
7[d]	[61], Fluid-11	41.71	62.3	424.82	0.970	0.516	3.0	0.820	32.20 (1)	1.91
8[d]	[57], Gas-5	30.29	61.8	403.70	0.971	0.552	2.0	0.660	4.17 (3)	0.01
9	[19], Sample-7	25.53	71.2	406.45	0.971	0.527	2.0	0.780	5.82 (1)	0.65
10	[64]	25.76	54.0	382.59	0.972	0.725	2.2	0.520	9.25 (1)	1.55
11[d]	[65]	44.40	66.4	435.93	0.965	0.629	4.0	0.790	2.61 (3)	0.01
12[d]	[62], Gas B	40.58	58.5	387.59	0.974	0.444	2.0	0.660	40.90 (1)	0.78
13	[66]	27.29	55.3	394.00	0.973	0.430	2.0	1.060	11.32 (1)	1.82
14	[5]	29.14	58.5	428.15	0.973	0.540	2.0	0.800	11.89 (2)	2.24
15	[25], PL-1	23.64	58.9	358.78	0.972	0.528	2.0	0.760	8.15 (1)	0.72
16	[25], PL-2	22.10	52.8	378.15	0.974	0.513	2.0	1.280	5.08 (1)	0.42
17	[25], PL-3	21.55	64.9	357.59	0.972	0.622	2.0	0.520	4.00 (1)	1.56
18	[25], PL-4	20.62	57.3	364.22	0.971	0.566	2.0	1.050	3.73 (1)	0.37
19	[25], PL-5	20.30	64.3	355.37	0.973	0.640	2.0	0.610	3.79 (1)	0.55
20	[25], PL-6	19.75	55.1	367.59	0.972	0.607	2.0	1.350	1.89 (1)	0.23
21	[67], CS-1	32.61	71.1	366.48	0.972	0.690	2.5	0.350	19.90 (1)	5.21
22	[67], CS-2	35.04	59.7	410.93	0.970	0.659	2.0	0.490	21.60 (1)	2.84
23	[67], CS-3	24.45	61.4	365.37	0.971	0.721	2.0	0.930	2.17 (1)	0.48
24	[21], NS-1	35.04	44.0[a]	410.43	0.971	0.659	2.0	0.490	21.60 (1)	2.83
25	[4], GOCW-7	33.62	60.5	358.70	0.973	0.575	2.5	1.050	23.90 (1)	2.50
26	[68], Example-1	54.92	57.1	410.90	0.890	0.572	2.9	0.960	69.81 (1)	8.79
27	[68], Example-2	32.65	59.5	436.70	0.975	0.684	2.0	0.530	15.63 (1)	0.96
28	[68], Example-3	26.26	58.4	393.20	0.973	0.604	2.0	1.000	4.75 (1)	0.63
29	[68], Example-4	28.34	59.0	377.60	0.971	0.586	2.1	0.830	11.84 (1)	0.73
30	[68], Example-5	21.27	56.4	377.60	0.970	0.716	2.0	1.340	1.69 (1)	0.43
31	JAPEX	29.81	58.9	402.59	0.972	0.641	2.0	0.570	6.67 (3)	0.06

[a] As reported. All other API gravities are calculated from density at 288.15 K and 1.01325 bars.
[b] (1) is CVD liquid saturation (%), (2) is CCE liquid saturation (%), (3) is CCE relative volume (v/v).
[c] Deviation = Sum of absolute of (experimental value–predicted value)/number of data point.
[d] Gas condensates 6, 7, 8, 11, and 12 are near critical.

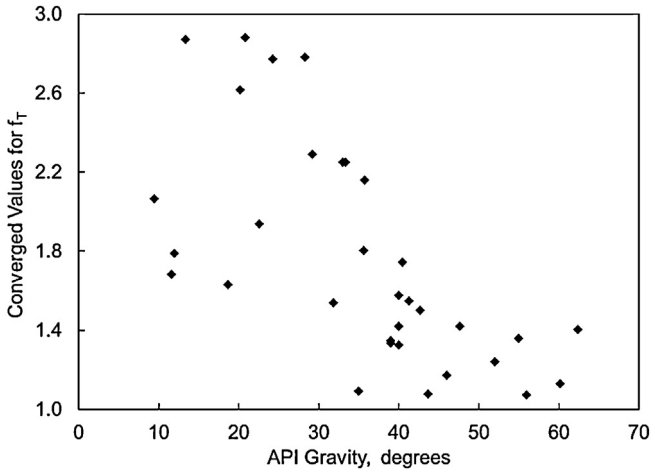

Fig. 20. Trend of the converged f_T values with respect to the API gravity. Heavier fluids tend to require more perturbation from *n*-alkanes.

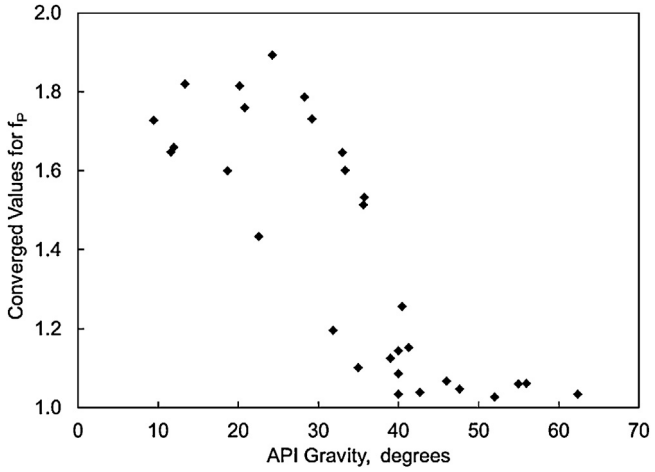

Fig. 21. Trend of the converged f_P values with respect to the API gravity. Heavier fluids tend to require more perturbation from *n*-alkanes.

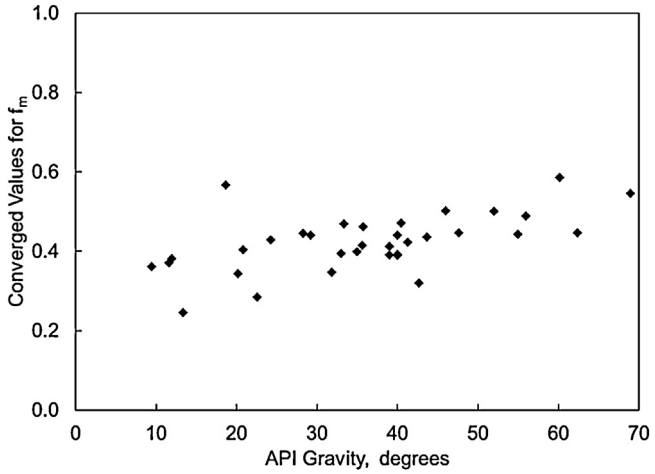

Fig. 22. Trend of the converged f_m values with respect to the API gravity. Heavier fluids tend to require more perturbation from *n*-alkanes.

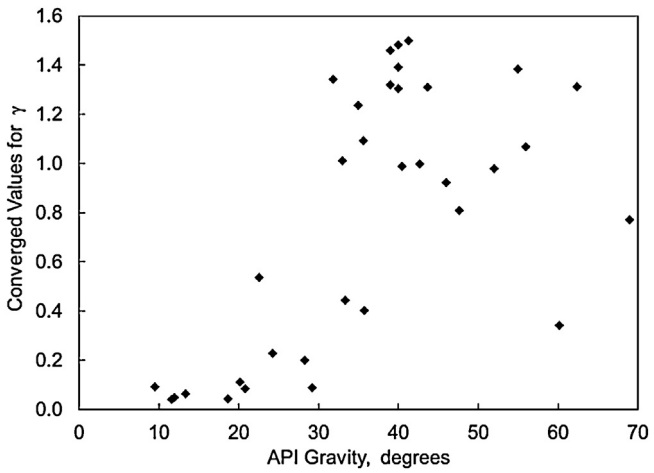

Fig. 23. The γ parameter becomes greater for lighter fluids. For heavy oils, variable perturbation from *n*-alkanes is less significant; the importance of the ψ and γ parameters diminishes as the API gravity becomes lower. For extra heavy oils, the PnA method reduces to the previous PnA method developed in Kumar and Okuno [3].

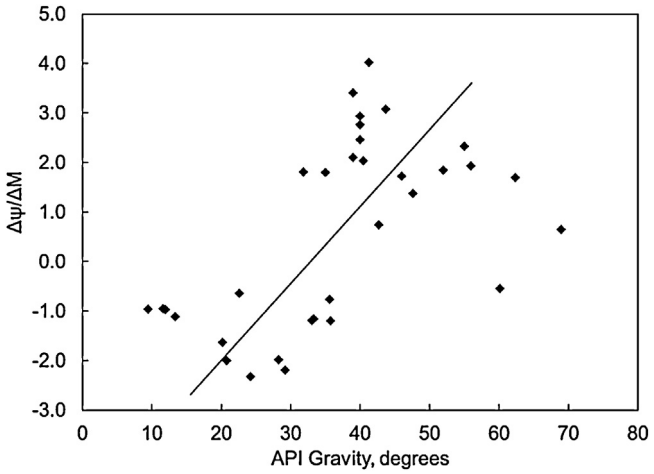

Fig. 24. Average gradient of ψ ($\Delta\psi/\Delta M$) for different fluids. This average gradient is calculated using ψ's and MWs for the lightest and heaviest pseudo components. The gradient is small for heavy fluids, and gradually increases as the API gravity increases.

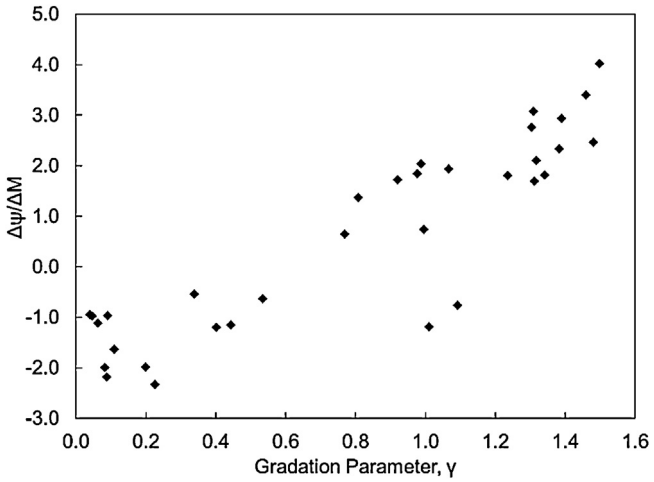

Fig. 25. Average gradient of ψ ($\Delta\psi/\Delta M$) with respect to γ. As γ increases, the average gradient also increases.

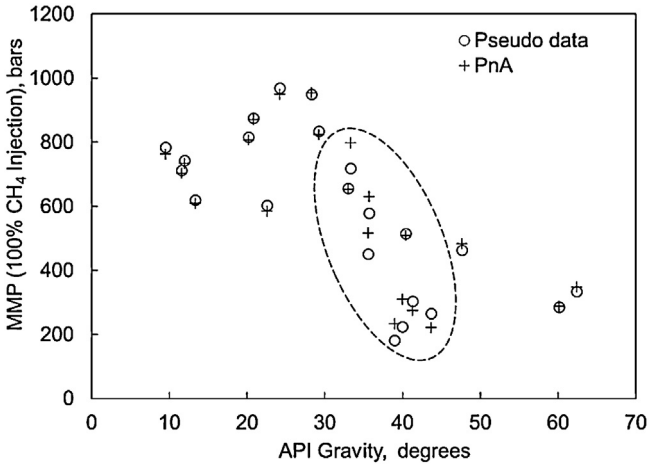

Fig. 26. Comparisons of C_1-MMPs for 22 oils in Table 4 using the PnA method and those from pseudo data. Good agreement is observed except for the API gravity range between 30 and 40. This is attributed to the discontinuity in the $CM_{w/o}V$ characterization used to generate pseudo data. PVTsim used in the $CM_{w/o}V$ gives two different characterization options, normal and heavy characterizations, based on an oil gravity criterion of 30°API.

30–40°API, however, have AD of 20% (encircled in Figs. 26 and 27). This is because of the discontinuity in the $CM_{w/o}V$ used to generate the pseudo data. PVTsim used in the $CM_{w/o}V$ gives two different characterization options, normal and heavy characterizations, based on an oil gravity criterion of 30°API. We observed that there can be significant differences in phase behavior predictions between these two characterization options around 30°API. Such a discontinuity in fluid characterization is undesirable considering the continuity of phase behavior (or, more fundamentally, the single-phase Gibbs free energy) in *P–T–x* space. The PnA method avoids the discontinuity by incorporating various physical considerations in the development as explained in the previous sections; the most important one is variable perturbation from *n*-alkanes for application to a wide variety of fluids. The AAD in C_1-MMPs and CO_2-MMPs for the 22 oils is approximately 7% using the extended PnA method.

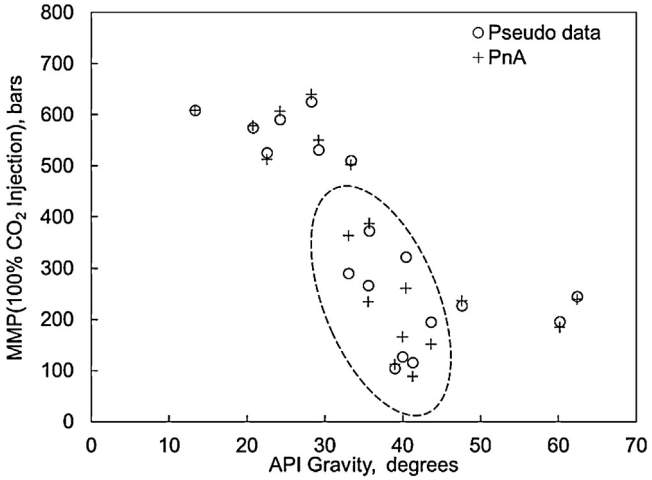

Fig. 27. Comparisons of CO_2-MMPs for 18 oils in Table 4 using the PnA method and those from pseudo data. Good agreement is observed except for the API gravity range between 30 and 40. This is attributed to the discontinuity in the $CM_{w/o}V$ characterization used to generate pseudo data. PVTsim used in the $CM_{w/o}V$ gives two different characterization options, normal and heavy characterizations, based on an oil gravity criterion of 30°API.

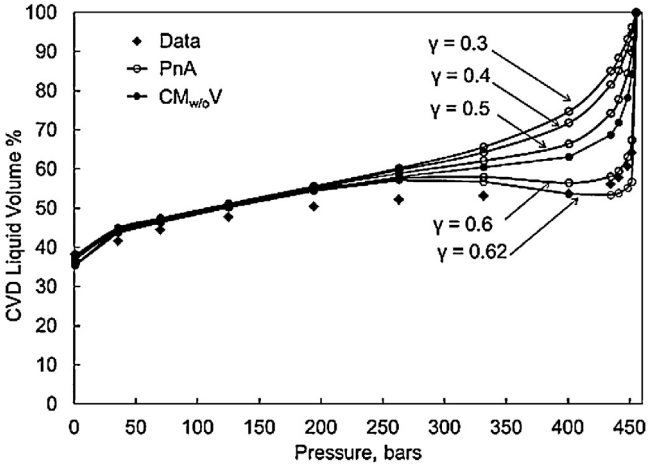

Fig. 28. CVD liquid saturation for volatile oil 1 given in Table 5. The reservoir temperature is 354.82 K. The oil has 12.92% C_{7+} mole fraction. The molecular weight of C_{7+} is 205 g/mol, and the overall molecular weight is 46.07 g/mol. Predictions are also presented using the PnA method with different γ values and $CM_{w/o}V$ methods. The γ parameter converges to 0.62 using the algorithm given in Section 3.4.

4.2.2. Volatile oils

We characterize the 12 volatile oils given in Table 5. The types of phase behavior predicted for the oils are presented in the table; liquid saturation in CVD and CCE, and relative volume in CCE are indicated as 1, 2, and 3, respectively, in Table 5. Table 5 also lists the limits of measured values in the experiments along with deviations of the predictions from data. Since these are volatile oils, liquid saturation is 100% at the bubble points. Liquid saturation data at lowest measured pressures are listed for data types 1 and 2. Relative volume data at lowest measured pressures are listed for data type 3. Using the PnA method, the AD is 3.7% in CVD liquid saturation prediction, and predictions of CCE relative volume are nearly perfect.

Figs. 28 and 29 compare the CVD liquid saturation curves for volatile oils 1 and 5, respectively. These oils were characterized using only saturation pressure data (see step 5 in the regression algorithm subsection). The PnA method yields the small AADs given in Table 5 for these oils even without using density data. The γ parameter converges to 0.62 using the algorithm given in Section 3.4. Fig. 28 also shows the CVD liquid saturation with the following γ values: 0.3, 0.4, 0.5, and 0.6. The liquid saturation curve varies

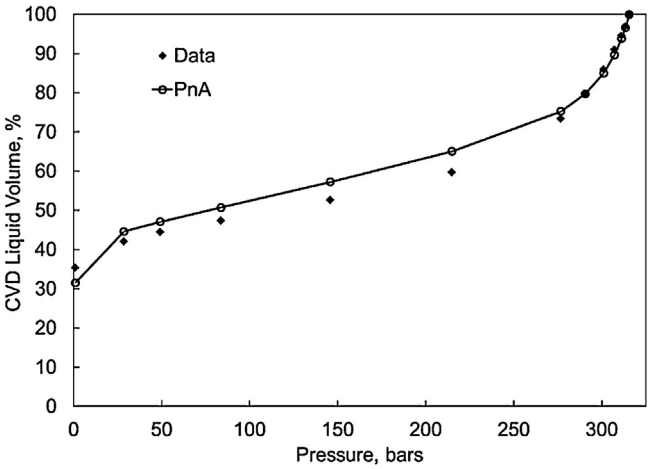

Fig. 29. CVD liquid saturation for volatile oil 5 given in Table 5. The reservoir temperature is 425.93 K. The oil has 17.2% C_{7+} mole fraction. The molecular weight of C_{7+} is 218 g/mol, and the overall molecular weight is 59.63 g/mol. Predicted values are also presented using the PnA methods.

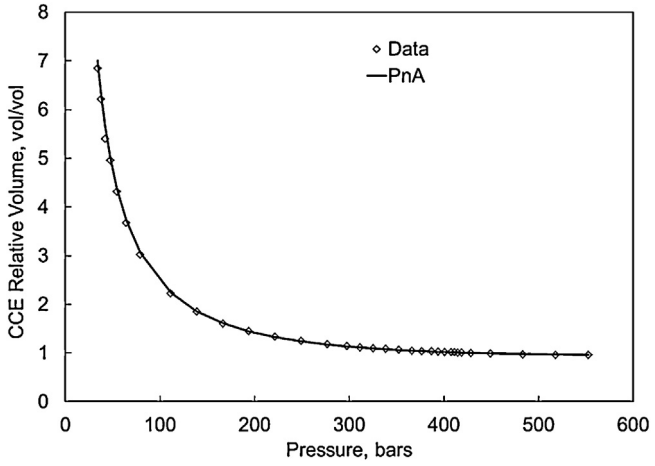

Fig. 30. CCE relative volume curve for volatile oil 6 given in Table 5. The reservoir temperature is 414.82 K. The oil has 19.0% C_{7+} mole fraction. The molecular weight of C_{7+} is 250 g/mol, and the overall molecular weight is 67.32 g/mol. Predicted values are also presented using the PnA methods.

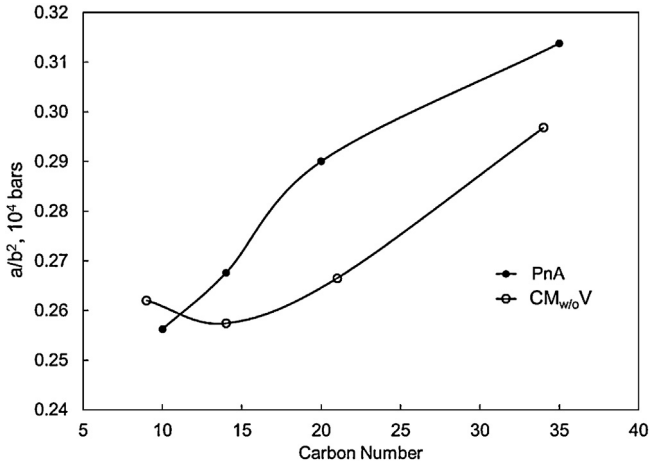

Fig. 32. Comparison of ψ trends for pseudo components for volatile oil 1 given in Table 5. Characterizations were made using the PnA and $CM_{w/o}V$ methods. The ψ trend for the PnA method exhibits a combined trend of the two model fluids in Fig. 13. The $CM_{w/o}V$ method results in the ψ trend that exhibits a minimum for the second lightest pseudo component.

monotonically with the γ parameter. As an example for CCE predictions, Fig. 30 compares the CCE relative volume for volatile oil 6. Nearly perfect prediction for the CCE relative volume is observed from the figure.

Fig. 28 also shows the liquid saturation curve using the $CM_{w/o}V$ with 12 components. The CN ranges for pseudo components in the PnA and $CM_{w/o}V$ are almost the same. For a fair comparison, density matching is not conducted for both cases (density matching actually deteriorates the CVD liquid saturation prediction using the $CM_{w/o}$ in this case). A large deviation is observed in the $CM_{w/o}V$ case for pressures between 250 bars and 455 bars.

To see the fundamental difference between the PnA and $CM_{w/o}V$ for volatile oil 1, Fig. 31 compares the a_i and b_i parameters for the four pseudo components in the two characterizations. It is difficult to find any abnormality in Fig. 31. However, Fig. 32 presents an important difference between the two characterizations in the ψ parameter, which was defined as a_i/b_i^2 before. The ψ trend for the PnA method exhibits a combined trend of the two model fluids in Fig. 13. The $CM_{w/o}V$ method results in the ψ trend that exhibits a minimum for the second lightest pseudo component. With this range of pseudo components' CNs, the ψ value for the second lightest pseudo component should not be less than that for the lightest pseudo component. A large deviation in the liquid saturation curve prediction around the saturation pressure is likely attributed to this ψ behavior for the $CM_{w/o}V$.

Volatile oil 12 in Table 5 is a near-critical fluid, for which CCE liquid saturation is predicted in Fig. 33. This oil is characterized at temperature of 371.6 K, and the critical temperature of the oil is 388.1 K. The PnA method is able to reproduce quantitatively the substantial sensitivity of liquid saturation to pressure. We also attempted to characterize this oil with $CM_{w/o}V$. However, the $CM_{w/o}V$ method predicted that the fluid is gas condensate rather than volatile oil. This is a common problem with conventional characterization methods for near critical fluids [61].

4.2.3. Gas condensates

The 31 gas condensates listed in Table 6 include a wide MW range from 19.75 to 54.92. Gas condensates 6, 7, 8, 11, and 12 are near critical. As indicated in Table 6, CVD liquid saturation curves (data type 1) are predicted for 26 gas condensates. CCE tests (data types 2 and 3) are predicted for the other five gas condensates. Characterization of the gas condensates does not use density data in

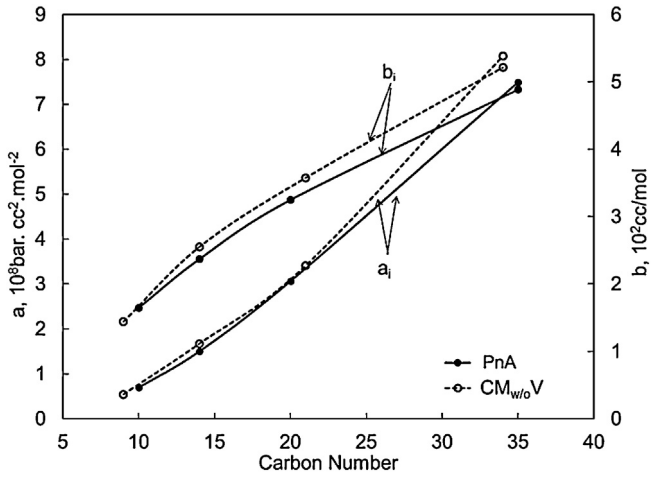

Fig. 31. Comparison of the a_i and b_i parameters for pseudo components for volatile oil 1 given in Table 5. Characterizations were made using the PnA and $CM_{w/o}V$ methods.

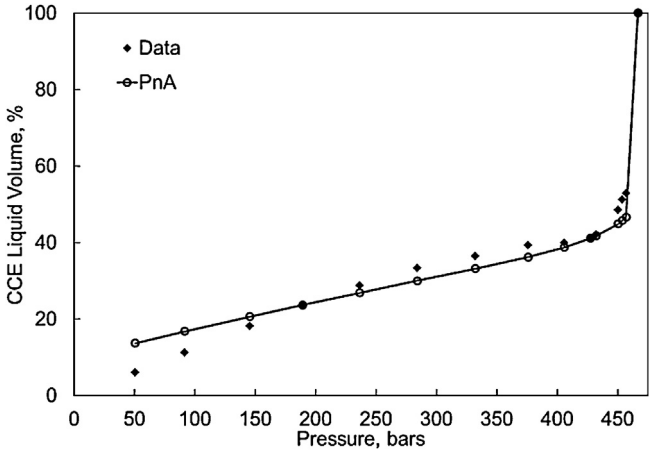

Fig. 33. CCE liquid saturation for near-critical volatile oil 12 given in Table 5. Predicted values are also presented using the PnA method. The reservoir temperature is 371.6 K, and the critical temperature is 388.1 K. The oil has 9.86% C_{7+} mole fraction. The molecular weight of the C_{7+} fraction is 192.8 g/mol, and the overall molecular weight is 37.94 g/mol.

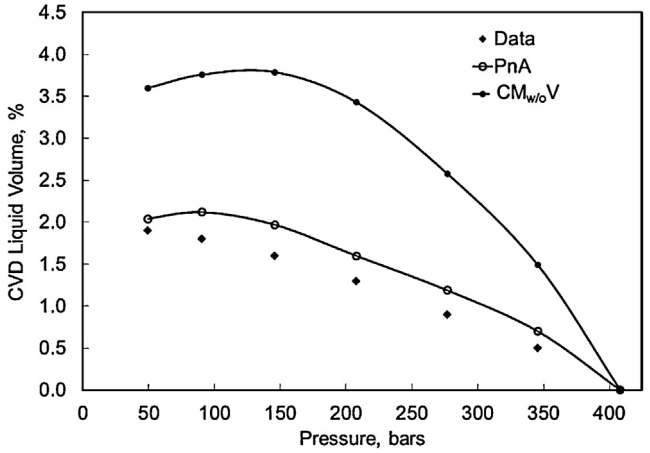

Fig. 34. CVD liquid saturation for gas condensate 20 given in Table 6 at 367.6 K. Predictions from $CM_{w/o}V$ with four pseudo components and from the PnA method are also presented. The gas condensate has 1.62% C_{7+} mole fraction. The molecular weight of the C_{7+} fraction is 143 g/mol, and the overall molecular weight is 19.75 g/mol.

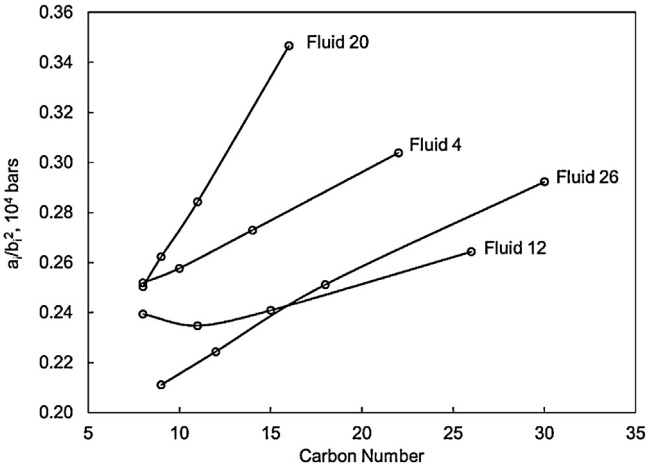

Fig. 36. Trends of ψ for gas condensates 4, 12, 20, and 26 given in Table 6. For gas condensates, the CN range of pseudo components is narrow. Therefore, ψ trends are increasing as shown in Fig. 13. In general, the slope of ψ becomes smaller as the CN range of pseudo components becomes wider.

regression due to low C_{7+} fractions. These gas condensates behave like light *n*-alkane mixtures, for which the PR EOS predicts densities accurately with the correlations of Kumar and Okuno [30]. The AAD for density predictions is less than 4% for the gas condensates given in Table 6.

Table 6 summarizes results for phase behavior predictions using the PnA method. For gas condensates, liquid saturation is zero at dew point. Hence, the maximum value in the experimental data is listed for each gas condensate, along with the AAD. The PnA method is successful for these gas condensates as indicated by the low AADs. As sample results, Figs. 34 and 35 depict CVD liquid saturation for gas condensates 20 and 5, respectively. The former exhibits low liquid saturation with a maximum of 1.89% at the lowest measured pressure. The latter exhibits a maximum saturation of 30.40% at a relatively high pressure in the two phase region. These figures also include the predictions from $CM_{w/o}V$ for comparison. The prediction from the $CM_{w/o}V$ method is in large error for the light gas condensate in Fig. 34. However, the $CM_{w/o}V$ and PnA methods give similar predictions for the rich gas condensate in Fig. 35. These results for gas condensates and volatile oils indicate that the PnA method is quantitatively accurate in prediction of quality lines and densities.

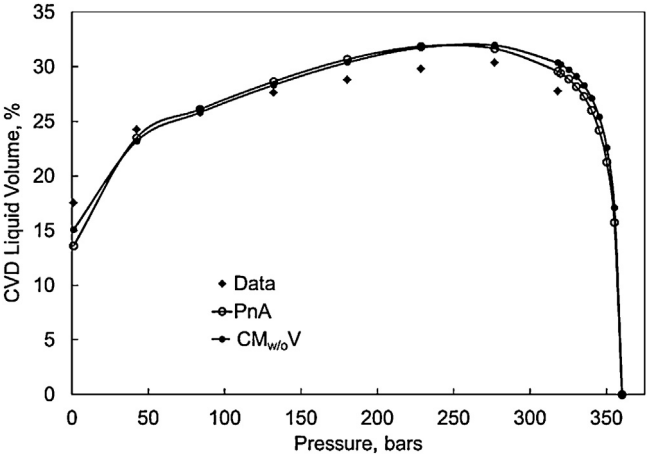

Fig. 35. CVD liquid saturation for gas condensate 5 given in Table 6 at 424.82 K. Predictions from $CM_{w/o}V$ with four pseudo components and from the PnA method are also presented. The gas condensate has 10.87% C_{7+} mole fraction. The molecular weight of the C_{7+} fraction is 173.0 g/mol, and the overall molecular weight is 40.77 g/mol.

Fig. 36 shows the ψ trends for gas condensates 4, 12, 20, and 26, for which the maximum liquid saturations are 25.00%, 40.90%, 1.89%, and 69.81%, respectively. The CN range of pseudo components is typically narrow for gas condensates, and the ψ parameter increases with CN as shown in Fig. 13. In general, the slope of ψ becomes smaller as the CN range of pseudo components becomes wider. The four pseudo components for gas condensate 20 are lighter than C_{20}. Hence, the sharply increasing trend is conceivable since the ψ parameter is sensitive to aromaticity in this CN region. Gas condensates 4 and 12 have CN ranges of C_8–C_{22} and C_8–C_{26}, respectively. The ψ parameters for these fluids exhibit convexity in the low CN region, which can be seen for *n*-alkanes in Fig. 13. Gas condensate 26 has the pseudo components in the CN range of C_9–C_{30}. Because of the wide CN range, the ψ parameter shows a combined trend of the two model fluids in Fig. 13.

Matching liquid saturation data can be difficult using the conventional fluid characterization methods. This is true especially when liquid saturation is sensitive to pressure and temperature (e.g., see Figs. 28, 33 and 35). Matching such liquid saturation data requires accurate prediction of dense quality lines and liquid densities (i.e., compositional and volumetric phase behaviors) along the experimental pressure path at a fixed temperature. However, the PR EOS is quite accurate in liquid density prediction for light fluids using the correlations of Kumar and Okuno [30]. Thus, adjustment of compositional phase behavior for the small C_{7+} fraction is crucial for reliable prediction of condensation/vaporization behavior of these fluids.

To show this, we characterize near-critical gas condensate 7 in Table 6 using the PnA and CM_wV methods. CVD liquid saturation curves from the two characterizations are compared with data points in Fig. 37. The CM_wV results in large deviations near the dew point. However, the two methods result in similar phase behavior for the C_{7+} fraction as shown in Fig. 38. The converged γ value for the PnA method is 0.820 as given in Table 6. The best match of the PnA characterization results in γ of 0.930. Fig. 38 shows that the two values of γ give essentially the same phase behavior of the C_{7+} fraction. These results indicate the significant sensitivity of liquid saturation to C_{7+} characterization in this case. *PVT* measurements for C_{7+} at the reservoir temperature 424.82 K and lower would not help because the three phase-envelopes nearly coincide there as shown in Fig. 38.

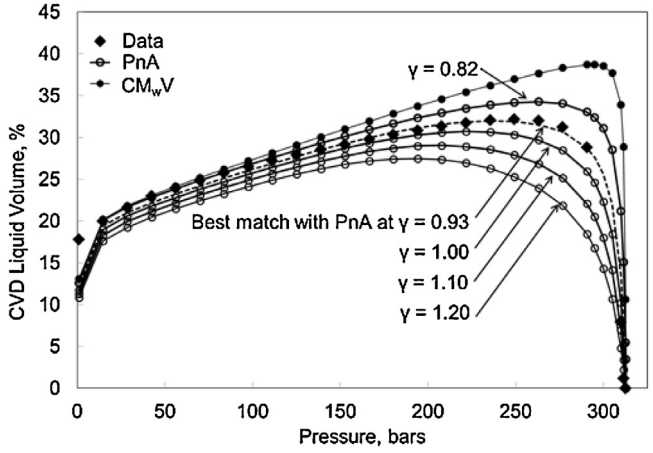

Fig. 37. CVD liquid saturation for near-critical gas condensate 7 given in Table 6 at 424.82 K. The gas condensate has 12.39% C_{7+} mole fraction. The molecular weight of the C_{7+} fraction is 158.23 g/mol, and the overall molecular weight is 41.71 g/mol. Predictions are presented using the CM_wV method and the PnA method with different γ values; 0.82, 0.93, 1.00, 1.10, and 1.20. The γ parameter converges to 0.82 using the algorithm given in Section 3.4.

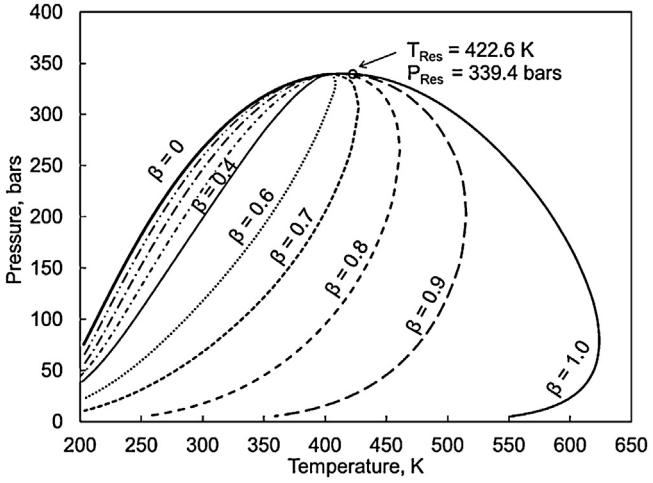

Fig. 39. Quality lines for near-critical gas condensate 6 given in Table 6. Vapor molar phase fractions (β) are shown beside the curves. The calculated critical temperature and critical pressure are 402.0 K and 339.2 bars, respectively. The reservoir temperature (T_{Res}) and pressure (P_{Res}) are is 422.6 K and 339.4 bars, respectively.

The PnA method is able to control gas condensate behavior by adjusting only one parameter (γ) to match the dew point. The adjustment changes phase behavior predictions systematically as shown in Figs. 37 and 38. Fig. 37 shows the CVD liquid saturation curves for different γ values. It is evident that the predicted curve changes monotonically with varying γ and systematically in pressure space.

Gas condensate 6 is another near-critical fluid, for which Fig. 39 shows quality lines (β is the vapor phase mole fraction). The calculated critical point is 402.0 K and 339.2 bars. The reservoir temperature and pressure are 422.6 K and 339.4 bars, respectively. Fig. 40 shows that the PnA method accurately predicts CVD liquid dropout, which results from the dense quality lines near the critical point.

4.2.4. Heavy oils

Oils heavier than 30°API listed in Table 4 are considered as heavy oils [26]. The present PnA method reduces to the previous PnA method developed for heavy oils [3] when γ is zero. As can be seen in Fig. 23, the γ values for extra-heavy oils of 10°API are nearly zero. The present PnA method performs similarly to the previous one for heavy oils. Our focus here is on the West Sak oil (oil 23 in Table 4), for which gas solubility data are available in the literature, and predictions of three hydrocarbon phases.

4.2.4.1. P–V predictions. For oil 23, the oleic phase saturations for two mixtures (60% CO_2 and 40% oil, and 80% CO_2 and 20% oil) are predicted at 299.81 K using the PnA method. Reasonable accuracy of the PnA method is observed in Figs. 41 and 42. The AAD is 2.7% for the 60% CO_2 mixture, and 5.6% for the 80% CO_2 mixture. Fig. 42 shows predictions with different γ values; 0.048, 0.8, 1.0, and 1.2. The converged γ value is 0.048 using the algorithm given in Section 3.4. A systematic change in predictions in pressure space is observed. The change is also monotonic with the γ parameter. With available phase saturation data, the optimum γ value can be easily selected using the PnA method.

Aghbash and Ahmadi [51] developed a 10-component fluid model for this oil. They used all non-zero BIPs. The PnA method does not require non-zero BIPs for hydrocarbon pairs to obtain similar phase behavior predictions. Fig. 43 compares the ψ parameters for pseudo components from Aghbash and Ahmadi [51] with those from the PnA method. The ψ parameter monotonically decreases with CN for the two cases, which is in line with our discussion for

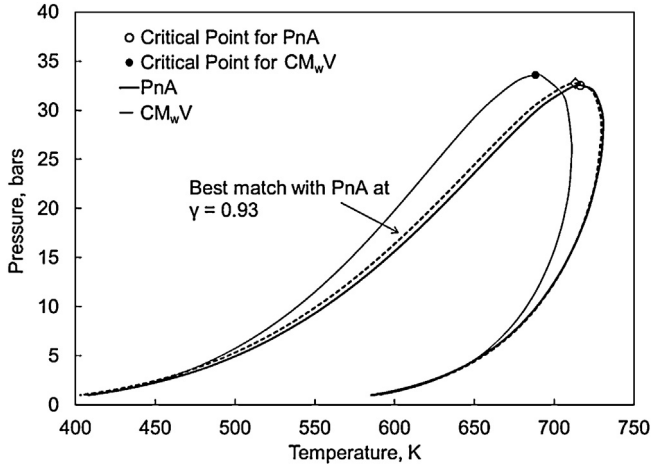

Fig. 38. *P–T* phase envelope for the C_{7+} fraction using the three fluid models shown in Fig. 37. The three models have similar phase behavior for the C_{7+} fraction. Liquid saturation given in Fig. 37 is sensitive to the C_{7+} phase behavior.

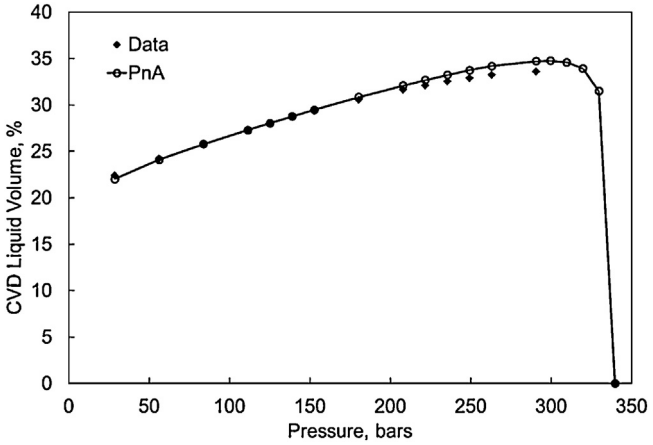

Fig. 40. CVD liquid saturation for near-critical gas condensate 6 given in Table 6 at 422.6 K. The gas condensate has 12.27% C_{7+} mole fraction. The molecular weight of the C_{7+} fraction is 154.93 g/mol, and the overall molecular weight is 39.23 g/mol.

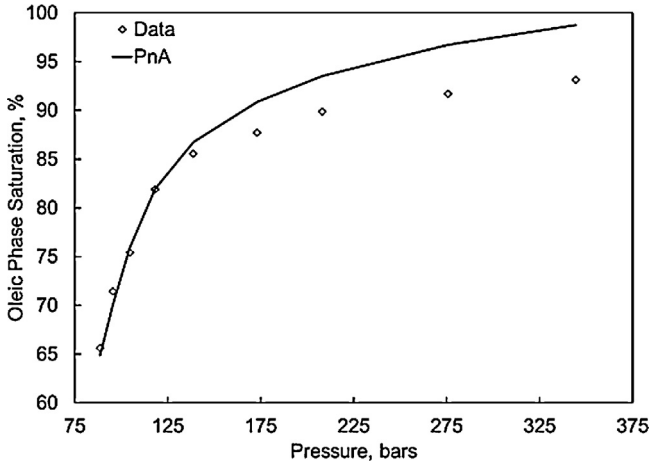

Fig. 41. Oleic phase saturation data and predictions using the PnA method for heavy oil 23 given in Table 4 [60] at 299.81 K. This is a mixture of 40% oil and 60% CO_2.

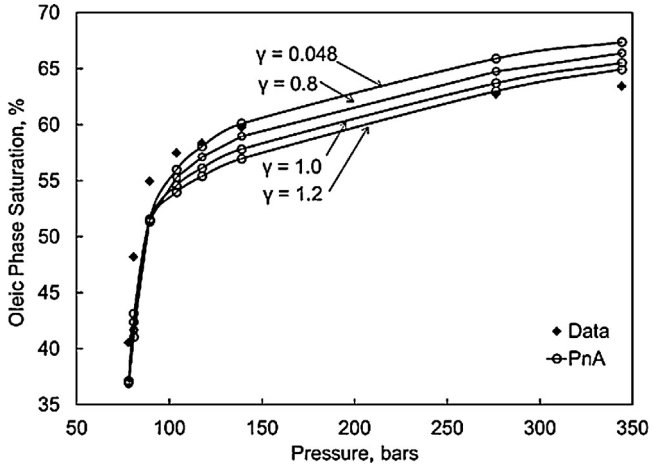

Fig. 42. Oleic phase saturation data and predictions using the PnA method for heavy oil 23 given in Table 4 [60] at 299.81 K. This is a mixture of 20% oil and 80% CO_2. The converged γ value is 0.048 using the algorithm given in Section 3.4.

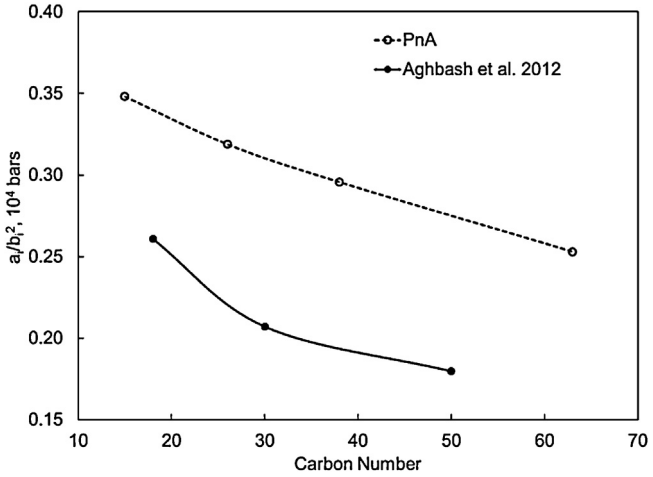

Fig. 43. The ψ parameter ($\psi = a_i/b_i^2$) for pseudo components for heavy oil 23 given in Table 4. Two characterizations compared are from Aghbash and Ahmadi [51] and the PnA method. The ψ parameter monotonically decreases with CN for the two cases, which is in line with our discussion for heavy oils in Fig. 13.

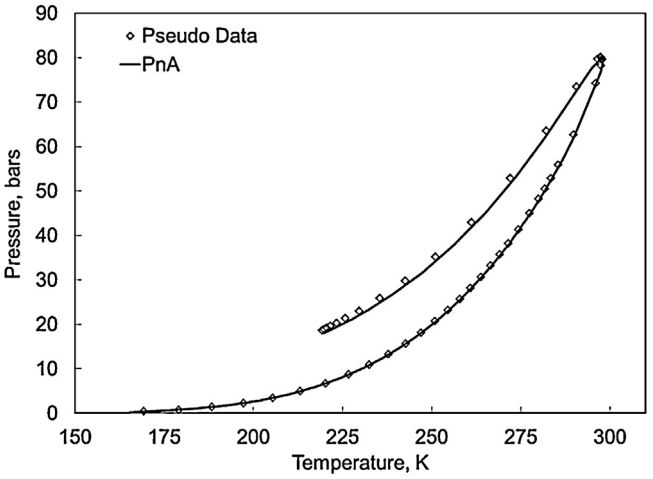

Fig. 44. Three-phase region from the PnA method is compared with pseudo data for a mixture of 20% oil 23 (Table 4) and 80% CO_2. Pseudo data has been created using 30 components (with 22 pseudo components) based on the conventional characterization using the PR EOS without volume shift.

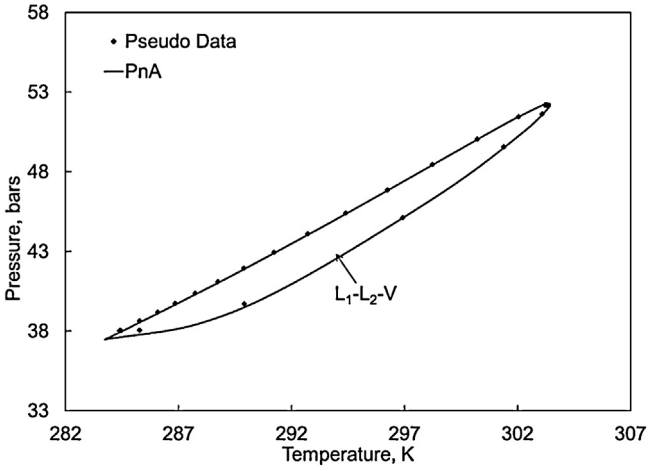

Fig. 45. Three-phase region from the PnA method is compared with pseudo data for a mixture of 10% oil 5 (Table 4) and 90% C_2. Pseudo data has been created using 30 components (with 22 pseudo components) based on the conventional characterization using the PR EOS without volume shift.

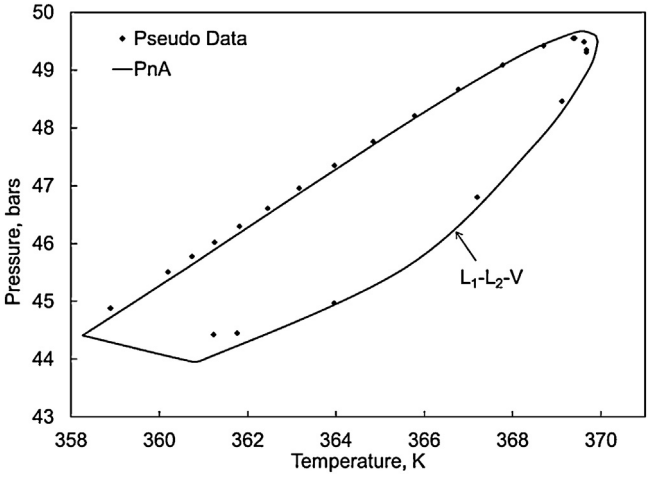

Fig. 46. Three-phase region from the PnA method is compared with pseudo data for a mixture of 10% oil 5 (Table 4) and 90% C_3. Pseudo data has been created using 30 components (with 22 pseudo components) based on the conventional characterization using the PR EOS without volume shift.

heavy oils in Fig. 13. The non-zero BIPs used in Aghbash and Ahmadi [51] likely did not cause absurd behavior of the Gibbs free energy in *P–T–x* space in this case. However, special care must be taken when BIPs are used in regression [5,9,38].

4.2.4.2. Three-phase predictions. Mixtures of oil and solvent can present complex three-hydrocarbon-phase behavior [52–54]. The three phases are the gaseous (V), oleic (L_1), and solvent-rich liquid (L_2) phases. Here, we compare three-phase predictions from the PnA method with pseudo data. Fig. 44 shows the three-phase envelope for a mixture of 80% CO_2 and 20% West Sak oil. Figs. 45 and 46 show the three-phase envelopes for two mixtures with oil 5 in Table 4; 90% C_2 and 10% oil 5, and 90% C_3 and 10% oil 5. Three-phase predictions from the PnA method nearly coincide with the pseudo data.

5. Conclusions

We first presented the effects of volume shift on phase behavior in *P–T–x* space when volume-shift parameters are used as regression parameters in fluid characterization. Then, the PnA method developed for heavy oils in our previous research was extended to characterize lighter fluids, such as gas condensates, volatile oils, and near-critical fluids. Extensive case studies using 77 different reservoir fluids demonstrated the universal applicability, reliability, robustness, and efficiency of the new PnA method. The PR EOS with the van der Waals mixing rules was used throughout the research. Conclusions are as follows:

1. Volume-shift parameters affect compositional phase behavior predictions when used as regression parameters in fluid characterization. *P–T–x* conditions used in laboratory measurements are only a small part of actual *P–T–x* conditions encountered in reservoir processes. Therefore, volume shift should be carefully performed in regression since it can substantially affect oil recovery predictions through altered phase behavior predictions in *P–T–x* space. The PnA method uses no volume shift, and properly couples volumetric and compositional phase behaviors.
2. T_C, P_C, and ω were perturbed to match the density trend curves with respect to CN for different levels of aromaticity presented in Yarborough [16]. Results show that uniform perturbation is appropriate for the CN range approximately higher than 20. Sharply increasing perturbation with CN is required for the lower CN range. This explains why the previous PnA method successfully used uniform perturbation for characterizing heavy oils, for which pseudo components' CNs are typically higher than 20. Case studies demonstrated that perturbation from *n*-alkanes depends on the CN range of pseudo components in the new PnA method.
3. The ψ parameter defined in Eq. (13) for the PR EOS is more sensitive to the level of aromaticity in the lower CN range than in the higher CN range. The ψ parameter increases with CN for fluids that have all pseudo components in the lower CN range, where sharply increasing perturbation with CN is required. The trend is the other way around for fluids that have all pseudo components in the higher CN range, where variable perturbation is less important. Mixed trends of the ψ parameter with respect to CN are expected for fluids that have pseudo components in the two CN ranges. Case studies confirmed this point. Conventional characterization methods can exhibit unexpected trends of the ψ parameter with respect to CN.
4. The regression algorithm developed in this research controls the trend of the ψ parameter with respect to CN using a fourth adjustment parameter γ. The algorithm also considers the size of composition space using the distribution function fitted to the composition data of the fluid to be characterized. Case studies showed the reliability and robustness of the algorithm for all fluids tested in this research. The algorithm written in FOTRAN takes less than two minutes on average per fluid using the Intel Core i7-960 processor at 3.20 GHz and 8.0 GB RAM.
5. The importance of the ψ and γ parameters diminishes as the API gravity decreases. For extra heavy oils, the new PnA method naturally reduces to the previous PnA method, where γ is zero.
6. The PnA method controls phase behavior predictions monotonically with parameter adjustments and systematically in *P–T–x* space. This was demonstrated by quantitative prediction of condensation/vaporization behavior of gas condensates and light oils and MMPs for various oil displacements, which can be difficult using conventional fluid characterization. Unlike the conventional methods, the PnA method uses only four adjustment parameters and incorporates physical considerations in parameter adjustment.
7. The PnA method requires no change in the thermodynamic model used, i.e., it can be readily implemented in existing software based on the PR EOS with the van der Waals mixing rules.

Acknowledgments

This research was funded by research grants from the Natural Sciences and Engineering Research Council of Canada (RGPIN 418266), Japan Petroleum Exploration Co., Ltd. (JAPEX), and Japan Canada Oil Sands Ltd. (JACOS). Ryosuke Okuno was awarded the 2012 SPE Petroleum Engineering Junior Faculty Research Initiation Award. Ashutosh Kumar was awarded the doctoral recruitment scholarship from the University of Alberta. We gratefully acknowledge these supports. We also thank Dr. Russell T. Johns for providing the PennPVT software.

Appendix A. Flow chart for the regression algorithm presented in Section 3.4.

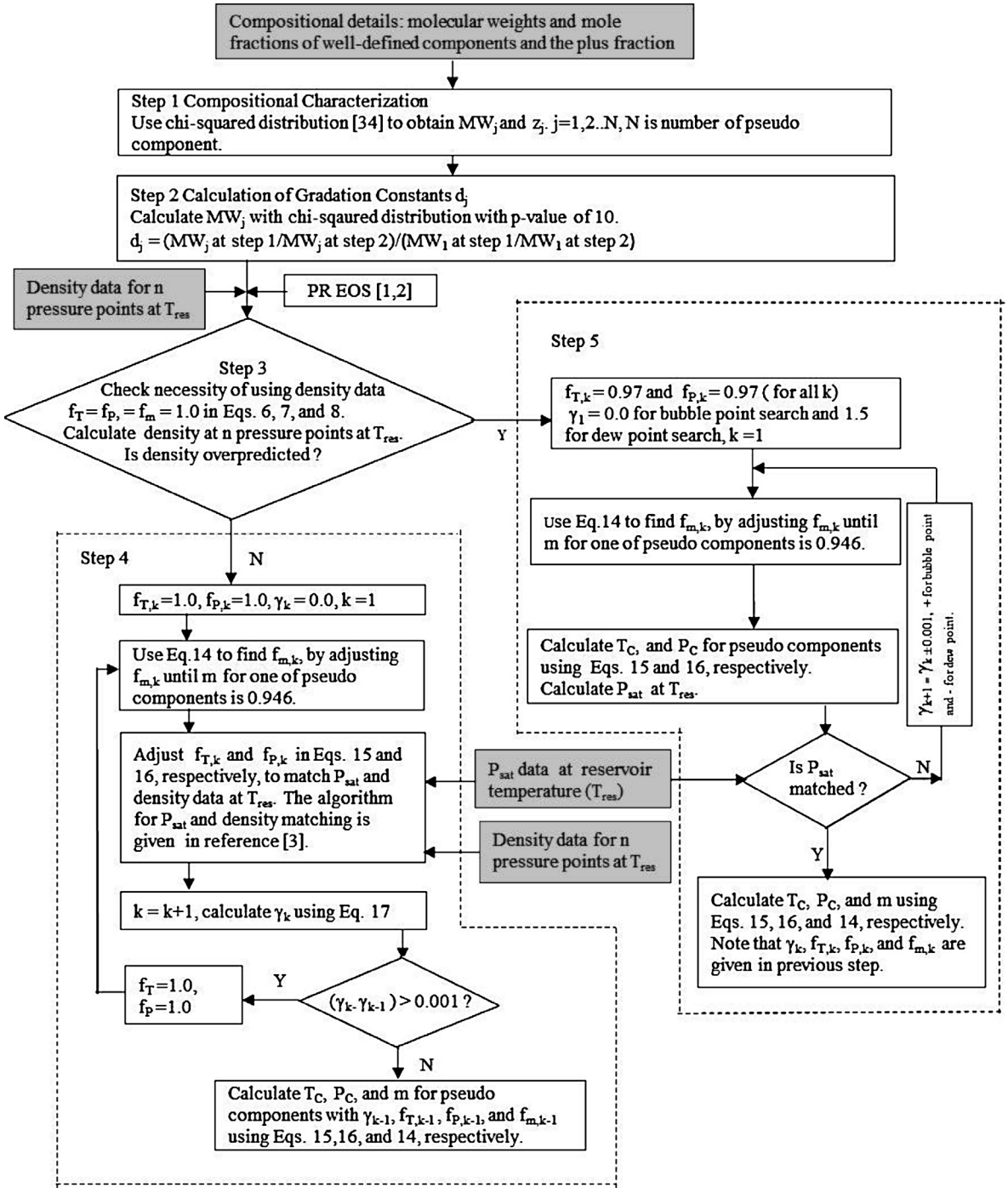

References

[1] D.-Y. Peng, D.B. Robinson, Ind. Eng. Chem. Fundam. 15 (1976) 59–64.
[2] D.-Y. Peng, D.B. Robinson, The Characterization of the Heptanes and Heavier Fractions for the GPA Peng-Robinson Programs. GPA Research Report RR-28, 1978.
[3] A. Kumar, R. Okuno, SPE Annual Technical Conference and Exhibition, San Antonio, Texas, 8–10 October, 2012, Paper SPE 159494-MS.
[4] C.H. Whitson, M.R. Brulè, Phase Behaviour Henry L. Doherty Series, vol. 20, SPE, Richardson, Texas, 2000.
[5] K.S. Pedersen, P.L. Christensen, Phase Behavior of Petroleum Reservoir Fluids, CRC Press, Taylor & Francis Group, Boca Raton, FL, USA, 2007.
[6] A. Peneloux, E. Rauzy, R. Fréze, Fluid Phase Equilib. 8 (1982) 7–23.
[7] B.S. Jhaveri, G.K. Youngren, SPE J. 3 (1988) 1033–1040.
[8] I. Søreide, Improved Phase Behavior Predictions of Petroleum Reservoir Fluids from a Cubic Equation of State, Norwegian University of Science and Technology, Trondheim, Norway, 1989 (Ph.D. dissertation).
[9] P. Wang, G.A. Pope, J. Petrol. Tech. 53 (2001) 74–81.
[10] C.S. Lolley, W.C. Richardson, International Thermal Operation and Heavy Oil Symposium, Bakersfield, California, 10–12 December, 1997, Paper SPE 37538.
[11] C.H. Whitson, SPE J. 23 (1984) 683–694.
[12] S.K. Stamataki, K.G. Magoulas, SPE International Symposium on Oilfield Chemistry, Houston, Texas, 13–16 February, 2001, Paper SPE 64996.
[13] F. Montel, P.L. Gouel, Annual Technical Conference and Exhibition, Houston, Texas, 16–19 September, 1984, Paper SPE 13119.

[14] C.F. Leibovici, Fluid Phase Equilib. 87 (1993) 189–197.
[15] F. Lomeland, O. Harstad, SPE Comput. Appl. 7 (1995) 38–43.
[16] L. Yarborough, Application of the generalized equation of state to petroleum reservoir fluids, equation of state in engineering and research, in: K.C. Choa, R.L. Robinson Jr. (Eds.), Advances in Chemistry Series, Am. Chem. Soc., vol. 182, 1978, pp. 386–439.
[17] A.S. Lawal, E.T. Van derLaan, R.K.M. Thambynaygam, Annual Technical Conference and Exhibition of the Society of Petroleum Engineers, Las Vegas, Nevada, 22–25 September, 1985, Paper SPE 14269.
[18] K.S. Pedersen, P. Thomassen, Aa. Fredenslund, AIChE Spring National Meeting, New Orleans, Louisiana, 6–10 March, 1988.
[19] T.M. Guo, L. Du, SPE e-library, 1989, Paper SPE 19374-MS.
[20] A. Peneloux, C. Jain, E. Behar, Annual Fall Technical Conference and Exhibition of the Society of Petroleum Engineers of AIME, Las Vegas, Nevada, 23–26 September, 1979, Paper SPE 8287.
[21] C.H. Whitson, S.B. Torp, J. Petrol. Tech. 35 (1983) 610–620.
[22] J.Y. Zuo, D. Zhang, SPE Asia Pacific Oil and Gas Conference and Exhibition, Brisbane, Australia, 16–18 October, 2000, Paper SPE 64520.
[23] A.A. Al-Meshari, W.D. McCain, SPE Technical Symposium of Saudi Arabia Section, Dhahran, Saudi Arabia, 21–23 May, 2006, Paper SPE 106338.
[24] R. Hosein, R.A. Dawe, J. Pet. Sci. Technol. 29 (2011) 817–823.
[25] R. Hosein, T. Jagai, R.A. Dawe, West Indian J. Eng. 35 (2013) 22–30.
[26] K. Krejbjerg, K.S. Pedersen, 57th Annual Technical Meeting of the Petroleum Society (Canadian International Petroleum Conference), Calgary, Canada, 13–15 June, 2006.
[27] M. Ghasemi, S.A. Alavian, C.H. Whitson, SPE Heavy Oil Conference and Exhibition held in Kuwait City, Kuwait, 12–24 December, 2011, Paper SPE148906-MS.
[28] J. Gregorowicz, T.W. de Loos, Ind. Eng. Chem. Res. 40 (2001) 444–451.
[29] V.I. Harismiadis, N.K. Koutras, D.P. Tassios, A.Z. Panagiotopoulos, Fluid Phase Equilib. 65 (1991) 1–18.
[30] A. Kumar, R. Okuno, Fluid Phase Equilib. 335 (2012) 46–59.
[31] K.S. Pitzer, J. Am. Chem. Soc. 77 (1995) 3427–3433.
[32] K.S. Pitzer, D.Z. Lippmann Jr., R.F. Curl, C.M. Huggins, D.E. Petersen, J. Am. Chem. Soc. 77 (1955) 3433–3440.
[33] S.E. Quiñones-Cisneros, C.K. Zéberg-Mikkelsen, A. Baylaucq, C. Boned, Int. J. Thermophys. 25 (2004) 1353–1366.
[34] S.E. Quiñones-Cisneros, A. Dalberg, E.H. Stenby, Pet. Sci. Technol. 22 (2004) 1309–1325.
[35] P.H. van Konynenburg, R.L. Scott, Philos, Trans. R. Soc. Lond. 298 (1980) 495–540.
[36] B. Nagy, U. Colombo, Fundamental Aspects of Petroleum Geochemistry, Elsevier, Amsterdam, 1967.
[37] J.-N. Jaubert, L. Avaullee, J.F. Souvay, J. Pet. Sci. Technol. 34 (2002) 65–107.
[38] A.M. Egwuenu, R.T. Johns, Y. Li, SPE Reservoir Eval. Eng. 11 (2008) 655–665.
[39] J.-N. Jaubert, L. Avaullee, C. Pierre, Ind. Eng. Chem. Res. 41 (2002) 303–310.
[40] S.L. Kokal, S.G. Sayegh, J. Pet. Sci. Eng. 9 (1993) 289–302.
[41] A. Yazdani, B.B. Maini, J. Can. Pet. Technol. 49 (2010) 9–14.
[42] R.C. Merrill, T.M.J. Newley, Fluid Phase Equilib. 82 (1993) 101–110.
[43] K.S. Pedersen, P. Thomassen, Aa. Fredenslund, Fluid Phase Equilib. 14 (1983) 209–218.
[44] K.S. Pedersen, P. Thomassen, Aa. Fredenslund, Ind. Eng. Chem. Proc. Des. Dev. 23 (1984) 163–170.
[45] K.S. Pedersen, P. Thomassen, Aa. Fredenslund, Characterization of Gas Condensate Mixtures Advances in Thermodynamics, vol. 1, Taylor & Francis, New York, 1989, pp. 137–152.
[46] K.S. Pedersen, A.L. Blilie, K.K. Meisingset, Ind. Eng. Chem. Res. 31 (1992) 1378–1384.
[47] K.S. Pedersen, J.J. Milter, H. Sørensen, SPE J. 9 (2004) 186–192.
[48] PVTsim 20.0. Calsep A/S, Lyngby, Denmark, 2011.
[49] K. Ahmadi, R.T. Johns, SPE J. 16 (2011) 733–742.
[50] PennPVT Toolkit, Gas Flooding Joint Industrial Project, Director: Dr. Russell T. Johns, EMS Energy Institute, The Pennsylvania State University, University Park, PA.
[51] V.N. Aghbash, M. Ahmadi, Western North American Regional Meeting, Bakersfield, California, 19-23 March, 2012, Paper SPE 1539 20.
[52] K.K. Mohanty, W.H. Masino Jr., T.D. Ma, L.J. Nash, SPE Res. Eng. 10 (1995) 214–221.
[53] I. Polishuk, J. Wisniak, H. Segura, Ind. Eng. Chem. Res. 43 (2004) 5957–5960.
[54] R. Okuno, R.T. Johns, K. Sepehrnoori, SPE J. 16 (2011) 751–767.
[55] M.F. Al-Ajmi, P. Tybjerg, C.P. Rasmussen, J. Azeem, SPE Middle East Oil and Gas Show and Conference, Manama, Bahrain, 25–28 September, 2011, Paper SPE 141241.
[56] S.E. Quiñones-Cisneros, S.I. Andersen, J. Creek, Energy Fuels 19 (2005) 1314–1320.
[57] K.H. Coats, G.T. Smart, SPE Res. Eng. 1 (1986) 277–299.
[58] S.E. Quiñones-Cisneros, C.K. Zéberg-Mikkelsen, E.H. Stenby, Fluid Phase Equilib. 212 (2003) 233–243.
[59] A.S. Cullick, F.N. Pebdani, A.K. Griewank, Ind. Eng. Chem. Res. 28 (1989) 340–347.
[60] G.D. Sharma, Development of Effective Gas Solvents Including Carbon Dioxide for the Improved Recovery of West Sak Oil, Report No. DOE/FE/61114-2, University of Alaska Fairbanks, Alaska, 1990.
[61] A. Al-Meshari, New Strategic Method to Tune Equation of State to Match Experimental Data for Compositional Simulation, Texas A&M University, Texas, 2004 (Ph.D. dissertation).
[62] D.A. McVay, Generalization of PVT Properties for Modified Black-Oil Simulation of Volatile and Gas Condensate Reservoirs, Texas A&M University, Texas, 1994 (Ph.D. dissertation).
[63] T. Yang, W.-D. Chan, T.M. Guo, Fluid Phase Equilib. 128 (1997) 183–197.
[64] O. Imo-Jack, Annual SPE International Conference and Exhibition, Tinapa-Calabar, Nigeria, 31 July–7 August, 2010, Paper SPE 140629.
[65] K.H. Coats, J. Petrol. Tech. 37 (1985) 1870–1880.
[66] A. Danesh, PVT and Phase Behavior of Petroleum Reservoir Fluids, Elsevier Science and Technology Books, 1998.
[67] D.C. Moore, Simulation of Gas-Condensate Reservoir Performance Using Schmidt-Wenzel Equation of State, Montana College of Mineral Science and Technology, Montana, 1989 (MSc thesis).
[68] J.K. Drohm, R.D. Trengove, W.H. Goldthrope, SPE Gas Technology Symposium, Dallas, Texas, 13–15 June, 1988, Paper SPE 17768.